



**LIFE 4 HEAT  
RECOVERY**

## **Report on urban heat island effect avoided – Action D.2**

---



**Low temperature, urban waste heat into district heating and cooling networks  
as a clean source of thermal energy  
LIFE4HeatRecovery**





**Project Title:** Low temperature, urban waste heat into district heating and cooling networks as a clean source of thermal energy

**Project Acronym:** LIFE4HeatRecovery

**Deliverable Title:** Report on urban heat island effect avoided

**Lead beneficiary:** EURAC

**Marco Cozzini, EURAC**

**Date:** September 2023

This document has been produced in the context of the Life4HeatRecovery Project.

The project has received funding from the LIFE programme of the European Union under contract number LIFE17 CCM/IT/000085



## Table of Contents

1	Introduction.....	1
2	General concepts on urban climate .....	2
2.1	The urban boundary layer .....	2
2.2	Urban heat island (UHI) effect.....	5
3	Ospitaletto case.....	8
3.1	The climate of the Po valley .....	8
3.2	The town of Ospitaletto .....	9
3.3	The WUDAPT procedure .....	9
3.4	The WRF meteorological model.....	15
3.5	Study periods: cold and heat waves.....	19
3.6	Estimation of heating and cooling consumptions.....	22
3.7	Results .....	29
4	Heerlen case .....	49
5	Aalborg case .....	53
6	References.....	54

## 1 Introduction

This report of the LIFE4HeatRecovery project focuses on the evaluation of the Urban Heat Island (UHI) effect in the three cities involved in the project demonstration activities and on the analysis of the mitigation potential provided by waste heat recovery measures. From a practical point of view, the UHI effect consists in the difference in air temperature, at the level of the Urban Boundary Layer (UBL), between rural and urban areas.

A full analysis of this kind requires several steps. First, a preliminary analysis of the current urban situation is necessary, including typical climatic characteristics and an assessment of the UHI effect during a certain time of the year. One can then quantify the mean temperature difference between urban and surrounding (suburban or rural) areas depending on the season (e.g., winter/summer) and the time of the day (e.g., day/night). Finally, the most detailed approach includes the use of a meteorological model to reproduce the typical features of the urban climate in the sample city. This can also be used to test the impact of different scenarios of waste heat recovery.

In this work, the full approach shortly described above was applied to the case of Ospitaletto<sup>1</sup>, where, due to the warmer climate, even a limited UHI effect is expected to have a higher impact on citizens. For such case, the Weather Research and Forecasting (WRF) mesoscale meteorological model was used, coupled with the Building Effect Parametrization (BEP). This requires the identification of simulation periods. By analyzing temperature data of selected meteorological stations, one can select winter and summer periods, focusing respectively on heating consumption and on cooling consumption in different scenarios. Based on the selected periods, the inputs needed to run the model can be prepared. Urban land cover was here defined through the World Urban Database and Access Portal Tools (WUDAPT), a method able to classify the urban morphology into ten urban climate zones (UCZs), thanks to the combined use of Satellite Images and Google Earth. Other urban parameters, according to the NUDAPT (the National version of WUDAPT) procedure, were also computed. While the above input datasets remain constant if the simulation domain does not change, the estimation of energy consumption is an input that can vary according to different variables, such as the period of the year and the type of buildings. Not only the spatial distribution of consumption, but also the temporal distribution has been considered, proceeding to the creation of daily profiles of consumption, for the two periods of simulation. The results of the simulations provide insight into the UHI effect as well as estimates about its possible mitigation by substituting conventional heating and cooling systems with more energy efficient solutions. In particular, in the case of Ospitaletto, where a neutral-temperature district heating (DH) network – i.e., a cold network connected to decentralized heat pumps (HPs) – is installed, both heating and cooling could be managed simultaneously exploiting waste heat recycling. Including the cooling option (currently not yet active), the network would become a 5<sup>th</sup> generation district heating *and* cooling (5GDHC) network.

For the other cities involved in LIFE4HeatRecovery, namely Heerlen and Aalborg, the preliminary analysis showed smaller effects. This was particularly valid for Aalborg, a northern Danish city located nearby the sea, where the colder climate and wind effects prevent the formation of urban heat islands.

---

<sup>1</sup> The large work carried out for the Ospitaletto case was mostly carried out by Gianluca Borghi, during an internship at Eurac Research. He was supervised by the author of this report and by prof. Lorenzo Giovannini, of Trento University. Prof. Giovannini kindly made available the simulation models developed in his group, providing a crucial contribution for the detailed analysis. The work became the subject of the master thesis of Gianluca Borghi. Much of the content reported here is directly taken from this source.

For this Danish case, it was not considered useful to make any investigation beside the initial general climate assessment. For the case of Heerlen, since again no big effects could be expected, the perspective was broadened including two other larger Dutch cities (Amsterdam and Rotterdam), where literature data were available. On the other hand, a compared analysis of the building stock of these Dutch cases was carried out, assessing once more the impact of 5GDHC networks with respect to conventional cooling solution (as in Heerlen a network similar to the one of Ospitaletto is installed). The level of detail of the corresponding analysis is therefore lower than for Ospitaletto and not based on the full modelling procedure mentioned above.

In general, the UHI effect was found to be relatively small for the cities of the demo sites of LIFE4HeatRecovery. This is not surprising in view of either their small size (Ospitaletto) or their geographical location. Also the anthropogenic effect due to cooling did not exhibit large impacts *on average*. However, literature data for the large cities of Amsterdam and Rotterdam showed the existence of locally intense phenomena, where the introduction of innovative cooling solutions (like the one of 5GDHC) could play a non-negligible role. This subject is hence expected to deserve further attention in the future, especially for the summer season, in large cities, and in southern climates.

## 2 General concepts on urban climate

The climate in cities usually differs significantly from the average local conditions. According to Othmer, Schmitt, and Greiving, 2020, "cities and metropolitan areas, which are generally called the urban climate, cause local climatic effects, due to the different physical properties of their surfaces in comparison to the less built-up and greener surroundings". It will be increasingly important to plan the urban environment according to an assessment of urban climate dynamics, particularly in densely built-up and populated areas: climate change is expected to make this work even more important.

According to a revision of United Nations in 2018, it was estimated that 55% of the world's population lives in urban areas. Such percentage is expected to increase to 68% by 2050. Projections show that urbanization, the gradual shift in residence of the human population from rural to urban areas, combined with the overall growth of the world's population, could add another 2.5 billion people to urban areas by 2050, with close to 90% of this increase taking place in Asia and Africa (Nations, 2018). Focusing in particular on the Italian situation, currently the percentage of urban population is 71%, a bit lower than the percentage of European Union which is 75% (European, 2018). In general, the urban environment has become the most common ecosystem for humankind, thanks to the urbanization phenomenon.

Urban agglomerations have local effects on the microscale atmosphere and with their expansion, they can also locally intensify the effects of global climate change (Darmanto et al., 2019). For example, according to Rosenzweig, Antle, and Elliott, 2015, from 1961 to 2010, the mean annual temperatures in dozens major cities increased at rates of 0.12°C- 0.45°C per decade. The projection that, as a result of climate change, urban areas are meant to be increasingly warmer than surrounding rural areas, will have a significant impact on energy consumption for cooling, heat waves, sea breeze penetration, and urban extreme rainfall (Darmanto et al., 2019).

### 2.1 The urban boundary layer

In a scenario of urban climate, the concept of scale is essential to understanding the ways in which elements of the urban surface interact with adjacent atmospheric layers (Arnfield, 2003).

Linked to the issue of scale, the distinction between the Urban Canopy Layer (UCL) and the Urban Boundary Layer (UBL) is of primary importance. In the UCL (roughly from ground to roof level), processes of airflow and energy exchange are controlled by microscale, site-specific characteristics and processes. On the other hand, according to (Arnfield, 2003), "the UBL above roof level is that part of the planetary boundary layer whose characteristics are affected by the presence of the urban surface (or its land-use zones) below and it is a local-to mesoscale phenomenon controlled by processes operating at larger spatial and temporal scales". In other words, the distinction goes beyond mere scale: while the UBL is a mesoscale concept referring to that portion of the planetary boundary layer whose characteristics are affected by the presence of an urban area at its lower boundary, the UCL is a microscale concept, its climate being dominated by the nature of the immediate surroundings, especially site materials and geometry (Oke, 1976).

In Figure 1 schematic representations of the UBL and the UCL, highlighting the different scales to which they refer.

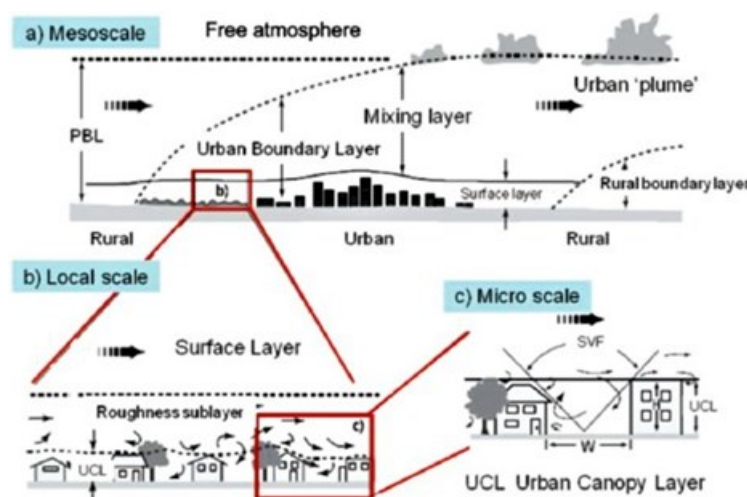


Figure 1. Schematic representation of the urban atmosphere illustrating the layers classification (Hove et al., 2010).

The different climatology between the urban climate and the surrounding areas is essentially attributable to changes in energy and water balance. In the next section such balances are discussed.

### 2.1.1 Urban energy balance

Oke, 1988 suggests, for the urban landscape, a useful approach able to estimate the energy balance for an imaginary volume within the urban canopy. The energy budget for such volume can be written as:

$$Q^* + Q_F = Q_H + Q_E + \Delta Q_S + \Delta Q_A$$

The net incoming amount of heat (left-hans side of the equation) is due to net solar radiation and heat production by human activity:

- $Q^*$  is the net all-wave radiation, which indicates the balance between the incoming and outgoing radiation fluxes (long-wave and short-wave);
- $Q_F$  denotes the anthropogenic energy release.

On the other side of the balance the following terms can be defined:

- $Q_H$  is the sensible heat, also called ‘atmospheric heating’, which is the sensible heat transferred to surrounding air and vanishing by wind and thermic airflow (Oke, 1988);
- $Q_E$  is the latent heat, mainly evapotranspiration;
- the two delta fluxes,  $\Delta Q_S$  and  $\Delta Q_A$ , represent the storage heat flux and the net advective flux.

In Figure 2, a graphical representation of the balance for a volume of air within the urban canopy is shown.

The **storage flux** is due to the heat stored within the building material. It is strongly dependent on solar variation and on the building material features. Obviously, at the same time, it is subject to a large uncertainty, due to the variety of materials present in a city, each one with its own thermal properties: it is not possible to measure it directly, but only through heat flux differences (Zonato, 2016).

Intensity of energy use, power generation and transportation system are the main causes of the **anthropogenic flux**. Then,  $Q_F$  is relatively high especially in the mid-winter months, due to intensive heating load, but also in the mid-summer months, due to a high air-conditioning load. The anthropogenic heat flux is a key-point in the urban energy balance also due the heat stored and re-radiated by massive and complex urban structures.

Since the parameters of the equation are functions of city location and characteristics, the energy balance inside a city varies with such parameters. In other words, UHI intensity is not spatially and temporally similar in different cities.

### 2.1.2 Urban water balance

(Oke, 1988) offers a definition of ‘urban blue bodies’ as “all the water bodies that can be found in urban areas, static or dynamic”. Blue bodies have influence on the urban environment, mostly due to the cooling ability of water bodies. The interaction with the mesoclimate is provided by evaporation or by the transfer of heat between air and water.

The urban water budget for an imaginary volume within the urban canopy can be written as (Grimmond and Oke, 2002):

$$p + I + F = E + r + \Delta A + \Delta S .$$

These variables are typically expressed in mm/h. Variables on the left hand side correspond to:

- $p$  is the precipitation
- $I$  is the piped water supply of the city;
- $F$  is the water vapour released due to anthropogenic activities, such as combustion.

Variables on the right hand side of the balance are defined as:

- $E$  is the evapotranspiration;
- $r$  is runoff;
- $\Delta A$  is the net advection of moisture for the volume;
- $\Delta S$  is the net change in water storage of the urban system, during the time period.

The water balance is linked to the energy balance through  $E$ , which is virtually proportional to  $Q_E$ , i.e. the latent heat flux.

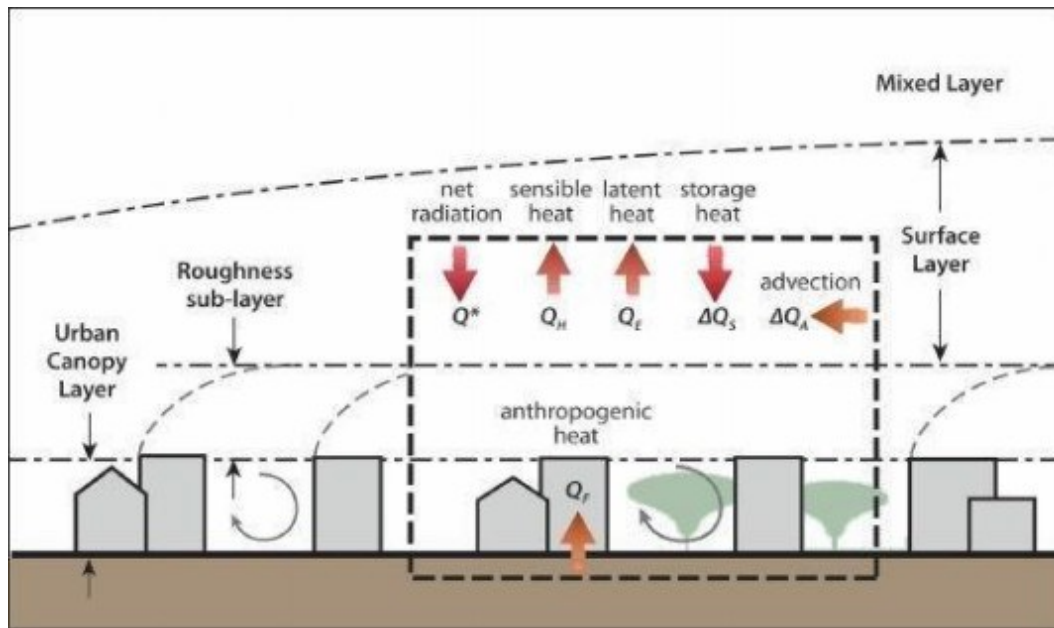


Figure 2. Heat balance around an urban canopy (Bhatt, 2016). The most external layer is the mixed layer: it results from convective air motions typically seen during the hottest hours of the day; the surface layer is the lowest part of atmospheric boundary layer, while the roughness sub-layer is defined as the region where the flow is influenced by the individual roughness elements such as stones, vegetation, trees, or buildings (Florens, Eiff, and Moulin, 2013).

## 2.2 Urban heat island (UHI) effect

The Urban Heat Island (UHI) effect refers to the warmer air temperatures in urban areas than in surrounding rural areas, due to urbanization (Rizwan, Dennis, and Chunho, 2008). As seen in the previous section, the energy balance within the city is generally different from the balance which takes place in the rural areas: the effects of the human activity on climate are various and interfere with the functioning of natural systems. Even just a single building significantly changes the surrounding environment: considering the energy transmission, for instance, on the one hand there is a reduction in the reception of solar radiation of shaded areas, on the other hand there is an increase in reflection by vertical surfaces. Moreover, the building will increase the surrounding air and ground temperature due to the heat losses from inside and wind reduction in the sheltered area.



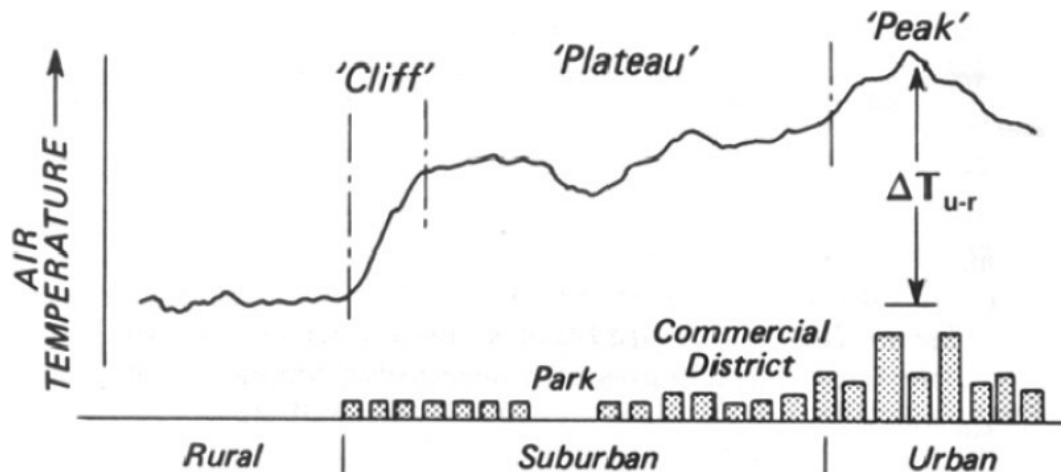


Figure 3. General section of a typical urban heat island (Oke, 1987).

The air temperature differences between urban and rural sites depend on factors as the local and synoptic weather, increasing particularly in relation with the occurrence of anticyclonic, clear sky, windless and cloudless conditions (Oke, 1982). The influence of wind speed and cloud cover on UHI have been reported in many studies. The results show a negative correlation with wind speed and cloud cover: the higher the wind speed and the cloud cover, the lower the UHI effect (Kim and Baik, 2005). On the other hand, the UHI effect has been reported to be positively correlated with the city population (Kim and Baik, 2005): increasing the number of people, anthropogenic releases grow and a larger concrete coverage is necessary in order to allow the people living in cities.

### 2.2.1 Causes of UHI effect

The various factors involved in the formation of UHIs can be categorized as controllable and uncontrollable. The controllable factors are mostly planning-related, which could be humanly controlled to some extent, while the uncontrollable factors are nature-related, which are beyond our control (Rizwan, Dennis, and Chunho, 2008). According to various authors the following are the main causes of the UHI effect:

- low amount of evapotranspiration because of less vegetation;
- absorption of solar radiation due to low albedo;
- hindrance to the flow of air because of higher rugosity;
- high amount of anthropogenic heat release.

However, there are also other factors which contribute to the formation of the UHI (Figure 4).

#### Low albedo materials

Albedo is defined as the ratio of the reflected solar radiation to the incident solar radiation. It depends on the arrangement of surfaces, materials, pavements, coatings, and has a direct impact on the formation of the microclimate. If the albedo of the urban surface is low, it will store more solar energy and the effect will be increasing the urban temperature. Building materials have also low thermal emissivity and, at the same time, a high thermal capacity: they tend to store a high amount of solar energy (in the form of heat) and release it over a long period of time.

#### Anthropogenic heat release

Since the heart of human activities and the main facilities reside within city centers, anthropogenic heat release is huge in these areas. During the winter, the main source of anthropogenic heat are the heating systems of the buildings. Furthermore, to provide comfort to the human beings at summertime, air conditioners are massively used. Air conditioners keep a building cool inside, but release the heat absorbed from inside, to the atmosphere. As a consequence, the outside environment is warmed, leading to the increasing of atmospheric temperature. Also vehicular traffic and, in general, urban human activities contribute to the release of anthropogenic heat that warms the urban environment.

### Urban geometry

The energy released by buildings inside street canyons tends to be trapped by the packed geometry of the urban area, causing an increase of temperature with respect to the atmosphere above roof level. Due to the presence of densely located buildings, wind velocity is reduced. As a result, the cooling effect by convection decreases and the heat trapped, cannot be blown out. On the other hand, such structure of the urban environment has an advantage: in the daytime promotes the creation of shadow zones which contribute to the surface and air temperatures reduction.

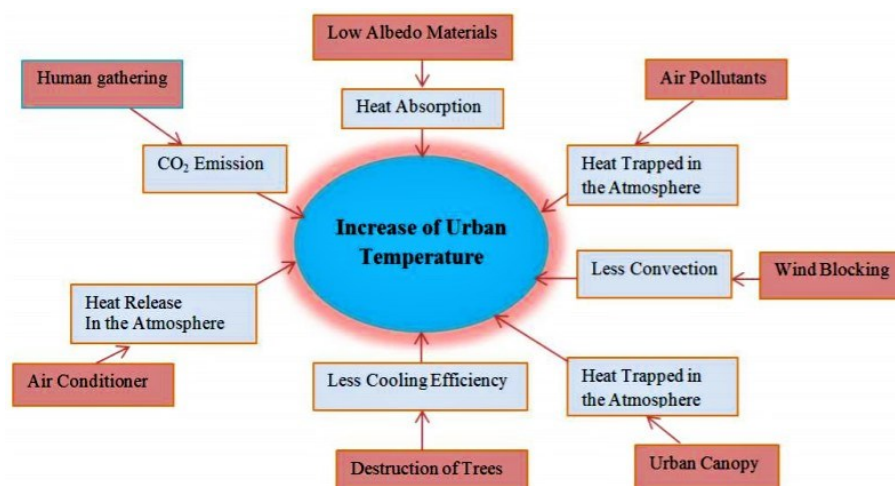


Figure 4. Schematic overview of the most relevant factors which are responsible for UHI generation (Nuruzzaman, 2015).

### 2.2.2 Mitigation strategies to reduce the UHI effect

UHI effect mitigation is necessary in order to face the negative effects that this phenomenon has on the quality of the urban environment and on the people's quality of life.

First of all, the primary consequence is related to human health: the increase of temperature and air pollution in the UBL tends to create discomfort, cardiovascular and respiratory problems, heart attacks, early deaths, especially in the elderly and children. A study about the correlation between air temperature and mortality during warm seasons (April to September) in two Portuguese sample cities, conducted by Almeida, Casimiro, and Analitis, 2013 has found that "the all-cause mortality in such regions increases by 3% and 5.6% with every 1°C rise of maximum daily temperature, respectively".

Not only the health aspect is interesting, but also the economic one. During the heat waves, an increase in energy consumption occurs: in summer, the peak electricity demand increases from 1.5% to 2% for each temperature increase of 0.6°C (Ranson, Morris, and Kats-Rubin, 2014).

According to the previous considerations, it is important to outline the effects and causes of the UHI, in order to find contrasting methods able to reduce the dangerous effect of this phenomenon. Sailor and Vasireddy, 2006 agree that the UHI effect mitigation could be reached in two ways: on the one hand by increasing the albedo of the urban surface, on the other hand, by increasing evapotranspiration. Albedo increases are generally accomplished through high albedo roofing and paving technologies. Increase in evapotranspiration is accomplished through a combination of decreasing the fraction of impervious surfaces and planting vegetation in urban areas. Mitigation strategies are generally focused on reducing summertime heat island magnitudes and may have less desirable effects during winter:

- **Cool roofs:** buildings and structures materials influence a lot the surface energy balance. The urban surfaces absorb large solar and infrared radiation; such absorbed energy is then dissipated in the environment through convective and radiative cooling processes, increasing ambient temperature. Since roofs occupy 20-25% of the total urban surface (Chen, 2013), a reduction in temperature of urban roofs would lead to direct benefits to single buildings and indirect benefits to the whole urban land. Cool roofs are made by materials with excellent reflective properties of visible radiation and high infrared emissivity.
- **Cool pavements:** urban horizontal surfaces are more affected by solar radiation, so they can reach quite high temperatures. Most of the urban area is covered by pavements: such surfaces, during the daytime absorb and accumulate solar energy that, during the night, is disposed of by cooling processes. Modifying pavements properties could represent an important factor on UHI mitigation. Santamouris et al., 2001 point out that while “roofs balance is influenced mainly by albedo and emissivity, pavements balance is influenced also by permeability, thermal capacity and convection”. Common materials are asphalt and concrete, but, using cool pavements like smooth, light-colored and flat surfaces allows a higher efficiency in reducing the heating effect.
- **Green areas, trees and vegetation:** mitigation of urban heat island can be carried out increasing the presence of parks and trees. Vegetation contributes to decrease the urban temperatures mainly thanks to evapotranspiration and shading, leading to the formation of cool islands in the city: planting even just a tree, in the tree proximity, solar radiation is reduced by 10-80% in summer and 10-30% in winter (Program, 2020). Close to a green area, sensible heat is lower because most of the radiation is used for water vaporization instead of increasing the temperature. Moreover a green area improves air quality: pollutants are absorbed or retained by vegetation, photosynthesis reduces carbon dioxide and the decrease of electrical energy for cooling demand reduces pollutant emissions and GHGs.
- **Green Roofs:** in an urban area, where buildings are so many and close, the space for parks and green areas might be not available. However, it is possible to exploit the large urban area occupied by the roofs of buildings, in order to realize green roofs, i.e. roofs covered by a vegetation layer.

### 3 Ospitaletto case

#### 3.1 The climate of the Po valley

The Po Valley is located between Alps and Apennines, in northern Italy. It extends approximately 650 km in the East-West direction, with an area of about 48.000 km<sup>2</sup>: it runs from the Western Alps to the Adriatic Sea.

It has a temperate sub-continental climate, with relatively cold winters and hot summers. The relative humidity is high throughout the year and causes strong storms and hailstorms in summer. The wind is normally weak, especially in the west-central part: being closed on three sides, the Po valley is one of the least windy areas in the world. The daily mean temperature during winter oscillates between 0°C and 4°C, while during summer the mean daily temperature goes from 25°C to 30°C<sup>2</sup>; during summer, with the presence of sub-tropical anticyclonic conditions, temperature can go beyond 38°C. Precipitation occurs mainly during spring and autumn, but stormy phenomena are frequent during summer.

The presence of mountains on the northern (Alps) and southern (Apennines) sides leads to frequent thermal inversion conditions, due to the drainage flows following the mountain slope. At the same time, the “Bora” wind coming from the north-east side can enter directly in this region. The Adriatic sea has a mitigation effect on the coastal areas, but it is too shallow and narrow to influence the internal area of the Po Valley<sup>3</sup>.

### 3.2 The town of Ospitaletto

Ospitaletto (45° 33 19 N, 10° 4 24 E) is a town of 14,947 inhabitants, located in the Lombardy region, province of Brescia, in the Po Valley, in the northern Italy. The territorial context where it is inserted is completely flat, with the city center situated at 154 m above the sea level. It is not a particularly touristic area, while the industrialized character prevails: in recent years a large amount of cultivated land has been replaced by buildings and important factories. Its strategic position is due to being close to two important highways (A4 and A35); the railway network also crosses the municipal area.

### 3.3 The WUDAPT procedure

The World Urban Database and Access Portal Tools (WUDAPT) project seeks to acquire and store urban data using a common framework and to link these data to available methods for climate analysis and for current and what-if scenario development (WUDAPT Global Initiative: Census of Global Cities). The focus is on function and morphology of urban environment and on the activities capable of influencing the energy balance. According to “An Introduction to the WUDAPT project”, “the WUDAPT initiative is a global, bottom up, self-organized effort to begin filling the data gaps needed to solve the global challenges of sustainable cities and communities, and as a guide to facilitate climate-based actions”. Relevant data in the study of urban climatic conditions are included in the acronym UFF (Urban Form and Function) for climate research reports. The urban form describes three aspects of the city: surface coverage, building materials properties, surfaces geometry (Bechtel et al., 2015). The WUDAPT approach allows a good level of customization and, if properly used, is expected to yield higher accuracy with respect to standard land-use classifications already available like the CORINE Land Cover database.

Given the urgent need for urban data to support climate research, WUDAPT has adopted a pragmatic approach to structure these data according to the level of detail. The characteristics of each level can be briefly summarized as follows:

- Level 0: regional and city scales
- Level 1: neighbourhood scale

---

<sup>2</sup> <https://sites.google.com/site/omnibuscience/meteorologia/meteogrammi-lombardia/meteo-cremasco/pianura-padana>

<sup>3</sup> <https://www.climatestotravel.com/climate/italy>

- Level 2: building scale

In this work, the lowest level of detail (L0) has been used. It consists of decomposing urban (and surrounding landscapes) into common Local Climate Zone (LCZ) types using local expertise, Landsat remote sensing data and software tools. The net result is a LCZ map of an urban region where each LCZ type is associated with a universal range of values that describe aspects of urban form and function.

One of the features that allowed the dissemination of the WUDAPT procedure is its wizard, which makes it reproducible and adaptable for different case studies. In order to elaborate level 0 data, the procedure illustrated by Bechtel et al.(2015) 1 has been followed. This procedure allows a land-use classification using 17 different classes (LCZs): ten of these classes, called Urban Climate Zones (UCZs), account for urban settlement types, while the remaining seven are referred to the rural environment (Figure 5). Each of the UCZs is associated with a combination of four parameters describing the urban morphology and the material properties with standard values. The four parameters are presented in Figure 6 (Stewart and Oke, 2012).










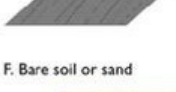

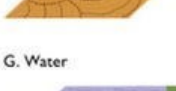




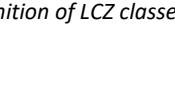
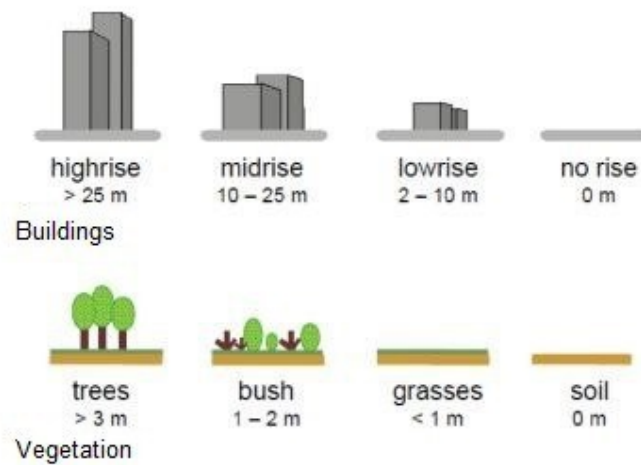
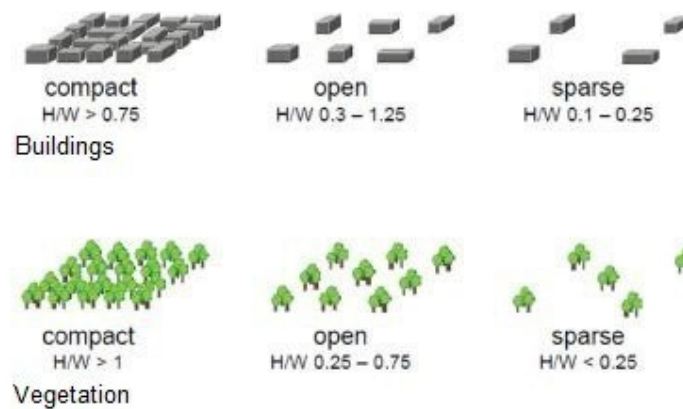
Built types	Definition	Land cover types	Definition
 <p>1. Compact high-rise</p>	Dense mix of tall buildings to tens of stories. Few or no trees. Land cover mostly paved. Concrete, steel, stone, and glass construction materials.	 <p>A. Dense trees</p>	Heavily wooded landscape of deciduous and/or evergreen trees. Land cover mostly pervious (low plants). Zone function is natural forest, tree cultivation, or urban park.
 <p>2. Compact midrise</p>	Dense mix of midrise buildings (3–9 stories). Few or no trees. Land cover mostly paved. Stone, brick, tile, and concrete construction materials.	 <p>B. Scattered trees</p>	Lightly wooded landscape of deciduous and/or evergreen trees. Land cover mostly pervious (low plants). Zone function is natural forest, tree cultivation, or urban park.
 <p>3. Compact low-rise</p>	Dense mix of low-rise buildings (1–3 stories). Few or no trees. Land cover mostly paved. Stone, brick, tile, and concrete construction materials.	 <p>C. Bush, scrub</p>	Open arrangement of bushes, shrubs, and short, woody trees. Land cover mostly pervious (bare soil or sand). Zone function is natural scrubland or agriculture.
 <p>4. Open high-rise</p>	Open arrangement of tall buildings to tens of stories. Abundance of pervious land cover (low plants, scattered trees). Concrete, steel, stone, and glass construction materials.	 <p>D. Low plants</p>	Featureless landscape of grass or herbaceous plants/crops. Few or no trees. Zone function is natural grassland, agriculture, or urban park.
 <p>5. Open midrise</p>	Open arrangement of midrise buildings (3–9 stories). Abundance of pervious land cover (low plants, scattered trees). Concrete, steel, stone, and glass construction materials.	 <p>E. Bare rock or paved</p>	Featureless landscape of rock or paved cover. Few or no trees or plants. Zone function is natural desert (rock) or urban transportation.
 <p>6. Open low-rise</p>	Open arrangement of low-rise buildings (1–3 stories). Abundance of pervious land cover (low plants, scattered trees). Wood, brick, stone, tile, and concrete construction materials.	 <p>F. Bare soil or sand</p>	Featureless landscape of soil or sand cover. Few or no trees or plants. Zone function is natural desert or agriculture.
 <p>7. Lightweight low-rise</p>	Dense mix of single-story buildings. Few or no trees. Land cover mostly hard-packed. Lightweight construction materials (e.g., wood, thatch, corrugated metal).	 <p>G. Water</p>	Large, open water bodies such as seas and lakes, or small bodies such as rivers, reservoirs, and lagoons.
 <p>8. Large low-rise</p>	Open arrangement of large low-rise buildings (1–3 stories). Few or no trees. Land cover mostly paved. Steel, concrete, metal, and stone construction materials.	<b>VARIABLE LAND COVER PROPERTIES</b>	
 <p>9. Sparsely built</p>	Sparse arrangement of small or medium-sized buildings in a natural setting. Abundance of pervious land cover (low plants, scattered trees).	Variable or ephemeral land cover properties that change significantly with synoptic weather patterns, agricultural practices, and/or seasonal cycles.	
 <p>10. Heavy industry</p>	Low-rise and midrise industrial structures (towers, tanks, stacks). Few or no trees. Land cover mostly paved or hard-packed. Metal, steel, and concrete construction materials.	<p>b. bare trees</p> <p>s. snow cover</p> <p>d. dry ground</p> <p>w. wet ground</p>	<p>Leafless deciduous trees (e.g., winter). Increased sky view factor. Reduced albedo.</p> <p>Snow cover &gt;10 cm in depth. Low admittance. High albedo.</p> <p>Parched soil. Low admittance. Large Bowen ratio. Increased albedo.</p> <p>Waterlogged soil. High admittance. Small Bowen ratio. Reduced albedo.</p>

Figure 5. Definition of LCZ classes (Stewart and Oke, 2012).

### Component 1: Height of Roughness Features



### Component 2: Packing of Roughness Features



### Component 3: Surface Cover Around Roughness Features



### Component 4: Thermal Admittance of Materials



Figure 6. Parameters, the combination of which, characterise the definition of LCZ (Stewart and Oke, 2012).

LCZs are referred to a scale ranging from microscale to mesoscale: the horizontal dimensions are between  $10^2$  m and  $10^4$  m. Grid resolution depends on the morphology of the case study: since this

work focuses on a relatively small urban area, the resolution chosen is rather high (30 m), in order to describe accurately morphological differences.

### 3.3.1 Definition of the Region of Interest (ROI) and creation of LCZ training areas

The first step is the ROI identification, i.e. the territory around the urban area to be analysed. The ROI is created in Google Earth Pro (Figure 7), drawing an area (known as a ‘polygon’) around the urban area. The ROI should contain the entire urbanized area, with a buffer of about 20 km around the area of the case study, in order to describe in a complete way the climatic conditions of the city.

Using Google Earth Pro, LCZ training areas for each class within the study area have been manually built. Training areas, characterized by homogeneous features in terms of morphology, density and materials, can describe each of the LCZ classes. Several zones are requested to represent truly the diversity of the urban landscape. Polygons dimensions have to be bigger than the resolution. The training areas used in this work are shown in Figure 7. The identified polygons were then imported in the SAGA (System for Automated Geoscientific Analyses) GIS (geographic information system), a free and open source software.

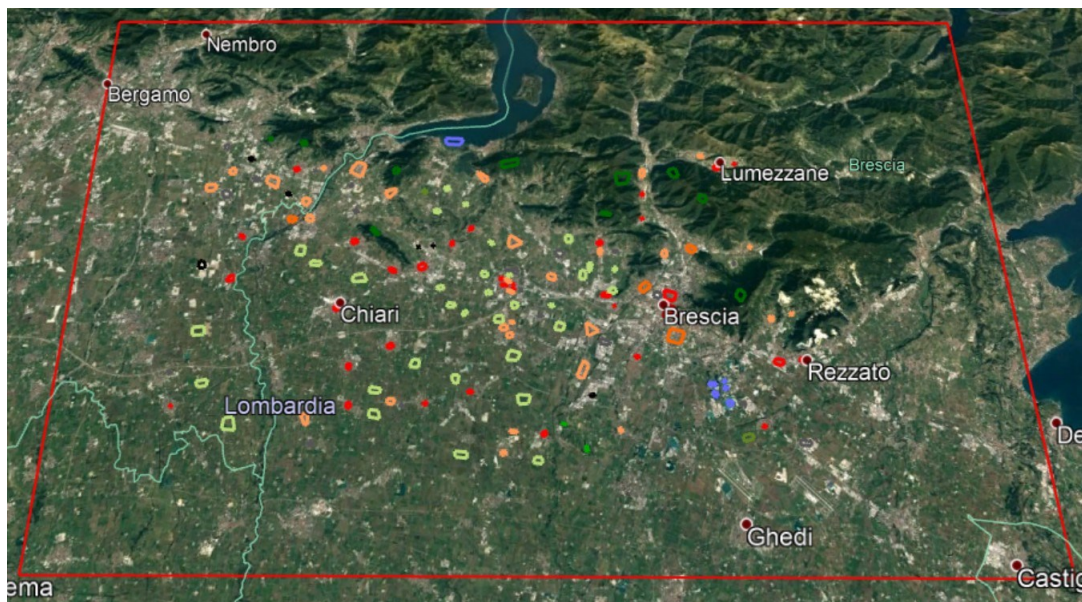


Figure 7. ROI and training areas individuation.

### 3.3.2 Satellite data and GIS

Satellite data for the study area were downloaded from Landsat8. Training areas need to be compared with them. In order to avoid systematic errors due to a single-day analysis, the images have to be related to different days in different seasons. The days chosen for this work are 31 January 2019, 26 March 2019 and 3 September 2019, with clear sky conditions (spatial resolution of 30 m). Nine images per period were chosen, each one representing a different wave-length of the radiation reflected by the surface.

Landsat8 satellite images were then used in the SAGA GIS software. SAGA GIS automatically classifies the pixels of the region of interest into LCZ types, superimposing the training areas imported from Google Earth to the satellite data. The tool *Local Climate Zone Classification* performs this automatic



process and provides as output the LCZ mapping. Finally, SAGA GIS is able to detect the different features within the study area (from the satellite data) and assigns to the pixels not covered with the training polygons the correct LCZ type.

### 3.3.3 Classification, iteration, and final definition of urban parameters

Once created the first raw classification, it is necessary to validate the accuracy of the classification: by examining the map, one can adjust the LCZ training areas, to account for misclassifications, repeating the process until a satisfactory result is reached. The accuracy of the final product is evaluated by comparing the predicted and observed LCZ type for selected areas.

Figure 8 shows the output of the WUDAPT classification for the ROI (about 2.000 km<sup>2</sup>), while in Figure 9 a zoom on Ospitaletto is shown.

After this process, the urban coverage for the study area is ready, in this case with a spatial resolution of 30 m. The LCZ map produced for the ROI with SAGA GIS has to be saved in an appropriate format (.txt), and transformed into an input for WPS (the WRF pre-processor, see below). The land-use map will have to be inserted into the meteorological model: before that, an interpolation is typically needed to match resolutions. For example, here the WUDAPT procedure was carried out with a 30 m resolution mask, while the meteorological model works with a resolution of 300 m. The interpolation is necessary in order to obtain customized UCPs (urban canopy parametrizations) for each model grid cell, overtaking the categorical definition of the LCZs (Zonato et al., 2020).

Just a few LCZs have been utilized, i.e. those considered most suitable to describe the morphology of the case study. Ospitaletto is a town with an extension of approximately 20 km<sup>2</sup>, inserted in a rural context (the 'Low plants' LCZ is the most typical one). As regards urban land-use, Table 1 reports an estimation of the percentage of area covered by each LCZ. The results show that Ospitaletto is inserted in a rural context, with an important industrial component also: concrete areas are wide and well distinguished from residential areas.

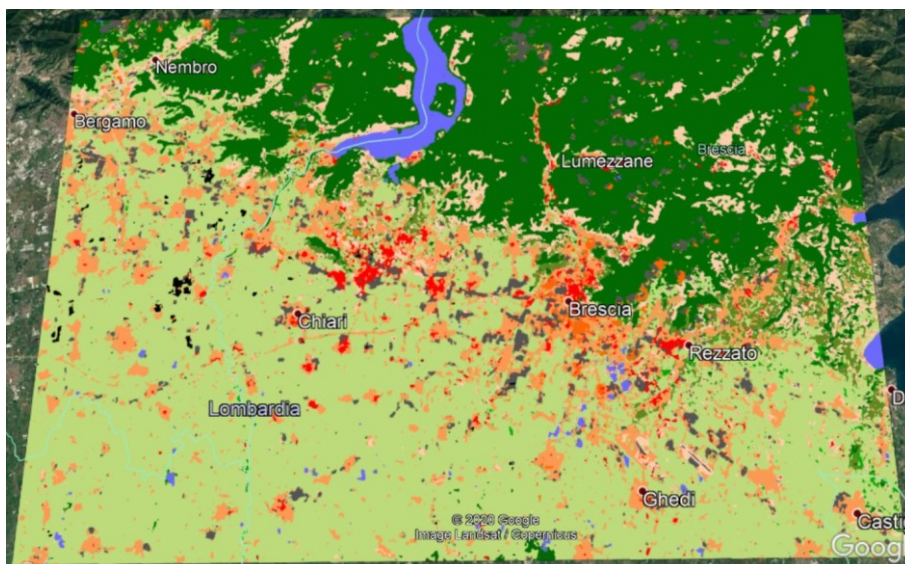


Figure 8. WUDAPT classification.

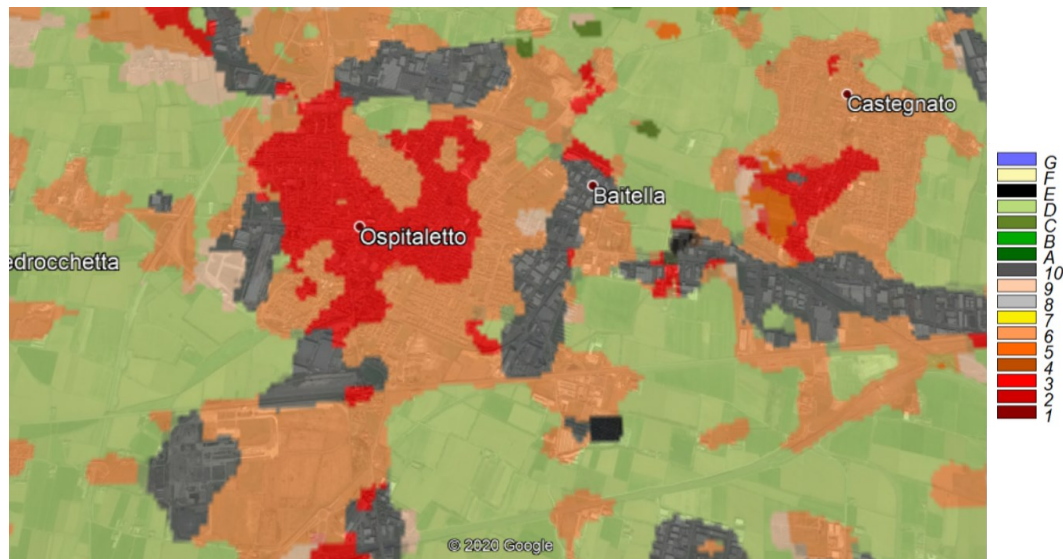


Figure 9. WUDAPT classification: focus on Ospitaletto. According to the classification of Figure 5, red is compact low-rise LCZ, orange is open low-rise LCZ, gray is heavy industry LCZ, and green is low plants LCZ.

Table 1. Urban coverage percentage.

UCZ	Description	Percentage of covered area
3	Compact low rise	25 %
6	Open low rise	40 %
10	Heavy industry	35 %

After the classification of the urban coverage into LCZ, it is necessary to assign to each class its own parameters. The variables requested, different for each class, are the urban fraction (i.e. fraction of urban landscape without vegetation), heat capacity, thermal conductivity, emissivity, roughness length and albedo for roof, ground and building walls, height distribution of the buildings (values are computed by steps of 3 m) and street and building width. Details on these values can be found in Borghi, 2020. Since no information on most of the parameters was available for the study area, the default values provided by the WRF mode (see below) were adopted (Zonato, 2016).

Values which were changed from the default setting are the height of the buildings: through the analysis of the height of buildings belonging to the city center (data available on the website <http://www.geoportale.regione.lombardia.it/download-dati>), the percentage distribution of the building height (every 3 m) could be computed.

### 3.4 The WRF meteorological model

Meteorological models are classified in different categories, according to the considered scale. A meteorological model is called *global* if its horizontal spatial domain covers the entire Earth, with horizontal grid spacing of the order of 10 20 km and 60-90 vertical levels (depending on the model). On the other hand, meteorological models at a *local* scale (LAM, Local Area Model) have a horizontal spatial domain covering only a portion of the Earth: in this way they allow to carry out simulations with greater resolution on areas of interest. The boundary conditions for the most external domain are provided by a global scale model, while, for the internal domains, boundary conditions are provided directly by the outer domain. This technique is defined *nesting* of computing domains: it provides the

identification of various domains with increasing resolution, centred on the area of interest. Anyway, a compromise between discretization and quality of prediction is necessary: a higher domain discretization leads to a higher quality of the prediction, but also to higher computational times.

Within the resolution of each domain, a multitude of physical phenomena occurs, very different from each other. Not all of them are solvable within the model itself (that is, some atmospheric processes cannot be solved explicitly at the spatial resolution with which meteorological models are usually used) and are therefore simply parameterized. Examples of processes to be parameterized can be turbulence in the boundary layer, heat and mass exchanges between the soil and the atmosphere, cloud micro-physics or radiation absorption by the atmosphere. In general, the meteorological model has a numerical structure, which solves numerically the conservation equations, and a series of parametrizations.

Initial conditions for meteorological models are given by different types of measures: ground-level observations, radio-soundings, wind profiles, satellite or aircraft observations. The higher the accuracy of the measures, the higher the reliability of the forecast.

Once one knows topography, land use and soil type, assigning boundary conditions means to assign values to variables on the grid nodes of the areas delimiting the boundary of the computing domain, in particular on the Earth's surface. For LAM, boundary conditions include also the value of the meteorological variables on the edge of the computational domain, provided by global models.

The Weather Research and Forecasting (WRF) model is a non-hydrostatic mesoscale numerical weather prediction model developed by the US National Center for Atmospheric Research (NCAR) (Skamarock, Klemp, and Dudhia, 2008). The WRF system contains two dynamical solvers, known as the ARW (Advanced Research WRF) and the NMM (Non-hydrostatic Mesoscale Model). In this work, the ARW-WRF core is used.

### 3.4.1 The WRF pre-processing system

The WRF Pre-processing System (WPS) is a set of three programs (see Figure 10) used to build the model, i.e. the configuration of computational domain, the assimilation of input data and the preparation of initial and boundary conditions.

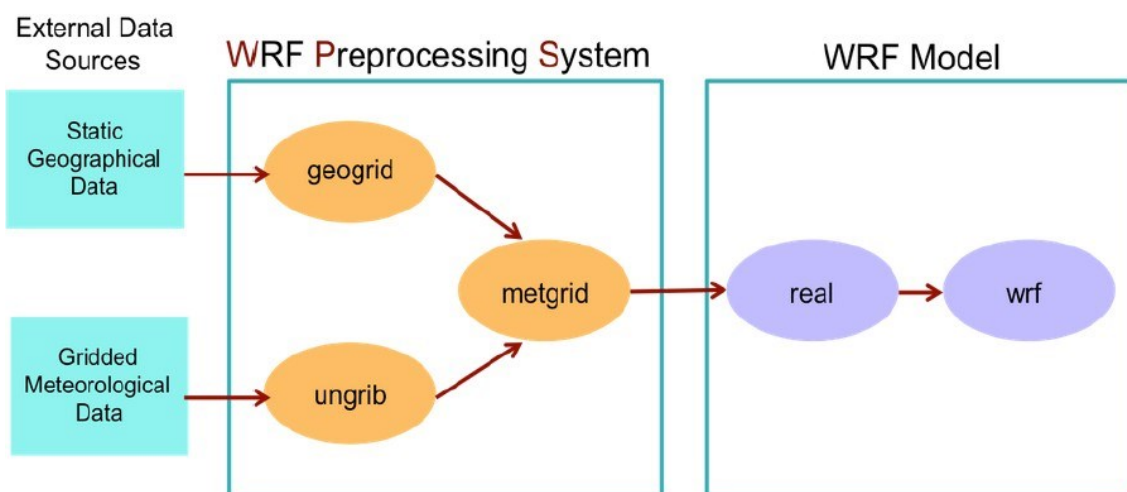


Figure 10. Schematic representation of WPS, WRF Pre-processing System.

The **geogrid** program is the first one, whose purpose is to define the simulation domains, and interpolate various terrestrial datasets to the model grids. With the aim of obtaining high resolution simulations, 4 computational domains centred on the area of interest have been used: the coordinates of the central point are  $lat = 45.8549$  and  $lon = 10.0807$ . The method used is called *nested domains* (Figure 11), where the resolution of a domain is equal to a third of that of the previous domain.

For a more detailed analysis of the urban context, the National Urban Data and Access Portal Tool (NUDAPT) procedure allows computing detailed physical and morphological parameters of the built environment (Figure 12). The GIS building information for Ospitaletto administrative boundaries have been obtained by Geoportal of the Lombardy Region. The municipality has been divided into square cells of a size of  $100\text{ m} \times 100\text{ m}$ . For each cell, the following variables have been computed:

- Building plan area fraction,  $\lambda_p = A_p/A_{tot}$ , where  $A_p$  is the plan (i.e., footprint) area of buildings and  $A_{tot}$  is the total paved area of the cell.
- Building surface to plan area ratio,  $\lambda_f = (A_p + A_w)/A_{tot}$ , where  $A_w$  is the wall surface area.
- Area-weighted average building height,  $h_{ave} = \sum_i h_i A_i / A_{tot}$ , where  $h_i$  and  $A_i$  are, respectively, the height and the footprint area of each building.
- Distribution of buildings heights every 3 m.

This preprocessing step also requires the insertion of the WUDAPT and NUDAPT classifications.

### WPS Domain Configuration

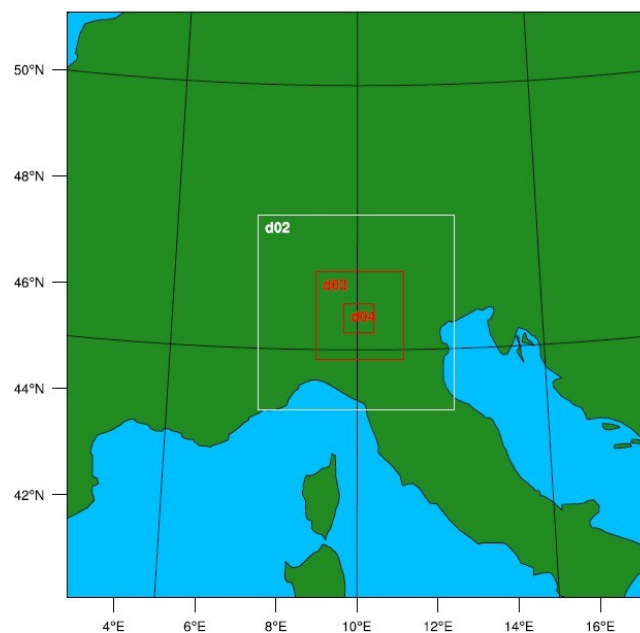


Figure 11. The four nested domains used for the numerical simulations.

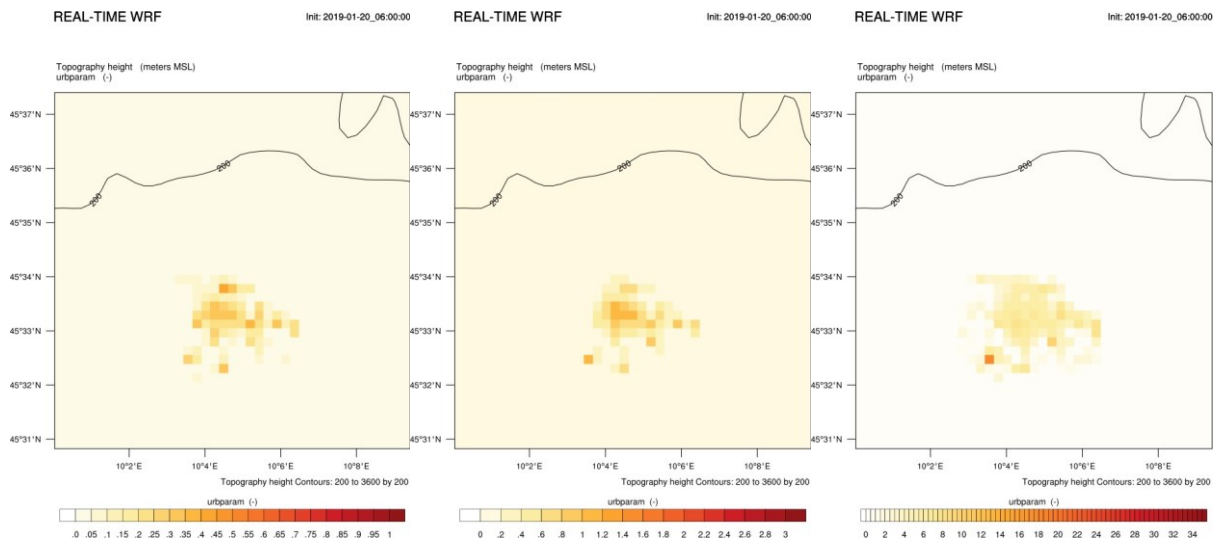


Figure 12. Urban morphology parameters distribution. Left panel: building plan area fraction,  $\lambda_p$ . Central panel: building surface to plan area ratio,  $\lambda_f$ . Right panel: area weighted mean building height,  $h_{ave}$ .

The second preprocessing program is called **ungrib**. Its purpose is to unpack GRIB (GRIB 1 and GRIB 2) meteorological data and pack them into an intermediate file format. GRIB is a WMO standard file format for storing regularly distributed (i.e. gridded) fields and contains meteorological/atmospheric data (Wang, 2014).

About the periods taken into account for the simulations, NCEP FNL (Final) Operational Global Analysis data, available every six hours and on a 0.25-degree by 0.25-degree resolution grid, have been downloaded. This product is given by the Global Data Assimilation System (GDAS), the system used by the model of the National Centers for Environmental Prediction (NCEP), which continuously collects observational data for many types of analysis. Such data are necessary in order to provide boundary conditions for domain d01 (parent domain) and initial conditions for all domains.

Finally, the third preprocessing program **metgrid** has the function to link the two kinds of data previously created in **geogrid** and **ungrib**. Such process involves a horizontal interpolation of meteorological data (downloaded by **ungrib**) within the domains identified through **geogrid**. The output of **metgrid** is a group of files named with the format "met\_em.d0n.yyyy-mm-dd\_hh:mm:ss.nc", where, for each domain  $n$  (with  $n = 1, \dots, 4$ ), the date and the hours of the interpolation are reported.

### 3.4.2 Physical parametrizations and BEP scheme

The Weather Research and Forecasting model is a numerical weather prediction and atmospheric simulation system designed for both research and operational applications. Its dynamics solver integrates compressible and non-hydrostatic Euler equations with several physical and dynamic options designed to phenomena at regional scale (Ribeiro et al., 2021). Due to the increasing interest on simulating the urban atmosphere and also due to the complex dynamics of the latter, developments have been integrated into the main WRF parameterizations (Salamanca et al., 2018).

The scheme used in this work to take into account the effect of the urban land-mask on the atmospheric dynamics is the Building Effect Parametrization (BEP).

The BEP urban physics scheme is an urban canopy model which is coupled with the land surface model in the WRF framework (Gohil and Jin, 2019). BEP provides the set of options to be selected for the study domain to parameterize the governing physical and dynamical interactions between the urban

surface and the atmosphere (Chen et al., 2011). BEP carefully considers the dynamical and radiative features of the urban canopy (i.e., roads, building rooftops and walls, concrete) using empirical expressions and thus has improved interpretation of physical and dynamical interactions. By dividing the urban canopy into several vertical layers and calculating an effective horizontal surface area at each vertical level using empirical expressions, BEP estimates surface energy fluxes, components of turbulent kinetic energy, the coefficients of absorptivity and reflectivity, and emissivity at that vertical level (Martilli, Clappier, and Rotach, 2002). Another feature of the BEP scheme is that it considers the impact of the shading induced by buildings heights within the urban canopy (Chen et al., 2011). As a result, it is expected to really well estimate heat fluxes and related properties, since BEP takes into account the influence of buildings and urban heterogeneities on the UCL.

### 3.5 Study periods: cold and heat waves

As reported in Chapter 2, the UHI is a typical phenomenon occurring in an urban environment. Unfortunately, there are not meteorological stations in Ospitaletto municipal boundaries, so, in order to make an analysis on temperature data, the closest stations available have been chosen: the urban one is located in the south of Brescia, close to Pastori High School, while the rural station is placed at Brescia airport (Brescia Ghedi), so the data have been downloaded by the Italian Air Force portal. Both the weather stations are shown in Figure 13. The distance between Ospitaletto and ITAS Pastori urban meteorological station is about 11 km, while the distance between Ospitaletto and Ghedi rural station is about 18 km. Both distances are acceptable and are expected to provide valid results. Comparing temperature data of such two meteorological stations located in the territory, it is possible to point out some evidences explained below.



Figure 13. Localization of urban and rural meteorological stations.

In this work, the UHI effect analysis is related to the implementation of a demo site in the already installed DH system in Ospitaletto municipality. Such innovative system, thanks to the installation of decentralized HPs at building sites, allows to work at low temperature, exploiting waste heat and renewable energy sources connected to the network.

Currently, in Ospitaletto, only a portion of heating demand is covered by such DH. For the future, however, a network expansion can be expected. It is hence interesting to consider a scenario where such technology is extended to cover the entire heating demand. Moreover, thanks to the possibility to connect to the network reversible heat pumps, it is also interesting to evaluate a scenario involving cooling demand as well. This is the reason why it has been considered appropriate to analyze critical periods characterized by particularly high and low temperatures, recorded at the two identified stations. These two periods have been called *cold wave* and *heat wave*. This analysis focuses on 2019 data.

### 3.5.1 Cold wave

During the winter season, the most important energy consumption is linked to the anthropogenic heat release. From this point of view, it is interesting to evaluate the effects of the implementation of the neutral-temperature DH system, able to recover waste heat, instead of the traditional current DH system.

The months of January and February 2019 have been characterized by a typical winter climate of the Po valley: cold and foggy weather, with high humidity. Focusing on the town of Ospitaletto, a data analysis for mean, minimum and maximum daily temperature of the urban meteorological station, for the months of January and February 2019, is shown in Figure 14. According to this figure, the minimum temperature was always lower than 7 °C, with a peak of 6 °C on 3rd January. At the same time, mean temperature has an important oscillation, with a minimum of 1 °C and a maximum of 12 °C. In view of these considerations, the study of the UHI effect for the town of Ospitaletto is focused on the time period that goes from 20th January 2019 to 24th January 2019: in this time frame the coldest temperature peak is not reached, but it represents a period of consecutive days on which temperatures are significantly low. Observing, for this period, almost identical meteorological conditions, the simulations cover the 36 hours ranging from 12:00 PM 21st January to 12:00 AM 23rd January. It was decided to start the simulations one day before the day of interest, because the first 12 hours of simulation are not taken into account: a spin-up time is requested in WRF for its initialization.

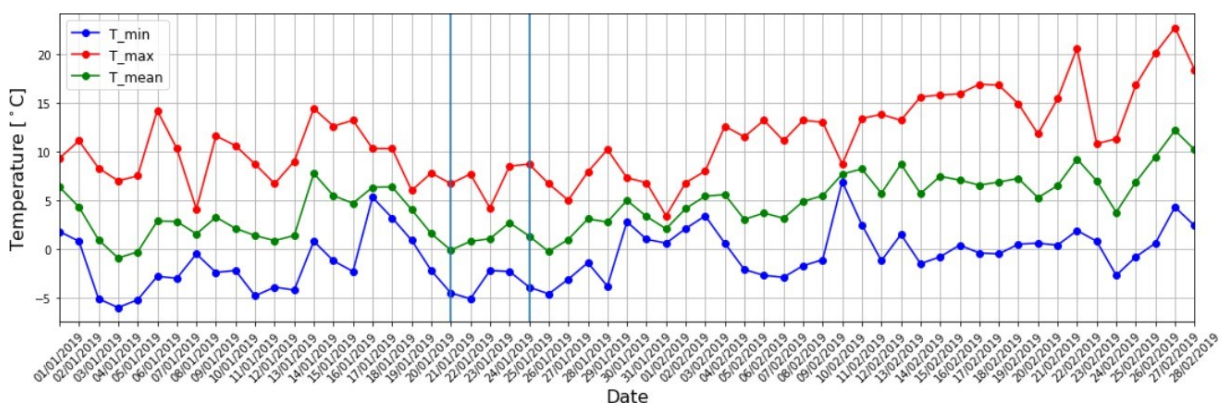


Figure 14. Daily minimum, mean, maximum temperature for the months of January and February 2019. Data come from a weather station situated in the urban area of Brescia (see text).

### 3.5.2 Heat wave

In order to evaluate the summer UHI effect for Ospitaletto, a period with extraordinary high temperatures has been chosen. This kind of phenomenon is called heat wave. In an article by Robinson, 2001, the heat waves are defined as "unusually high temperature events over consecutive days and may cause adverse impacts such as mortality": not only a significant concern for human health, but they also have effects on the frequency and intensity of extreme weather events (Woodward et al., 2014).

Analyzing the weather data of the urban meteorological station, in recent years, the months of July and August 2019 have been characterized by a subtropical air mass with stable conditions, on Italy. Focusing on the town of Ospitaletto, a data analysis for mean, minimum and maximum daily temperature for the months of July and August 2019 is shown in Figure 15. According this figure, the maximum temperature was always higher than 26 °C, with a peak of 39 °C on 25th July. At the same time, mean temperature lies always between 23 °C and 32 °C. In view of these considerations, the study of the UHI effect for the town of Ospitaletto, for the summer situation, is focused on the time period that goes from 22nd July 2019 to 25th July 2019. Observing, for this period, almost identical meteorological conditions, the simulations cover the 36 hours ranging from 12:00 PM 22nd July to 12:00 AM 24th July. As for the cold wayve, a spin-up time (about 12 hours) is requested for the WRF model, so it was decided to start the simulation 12 hours before the day analyzed.

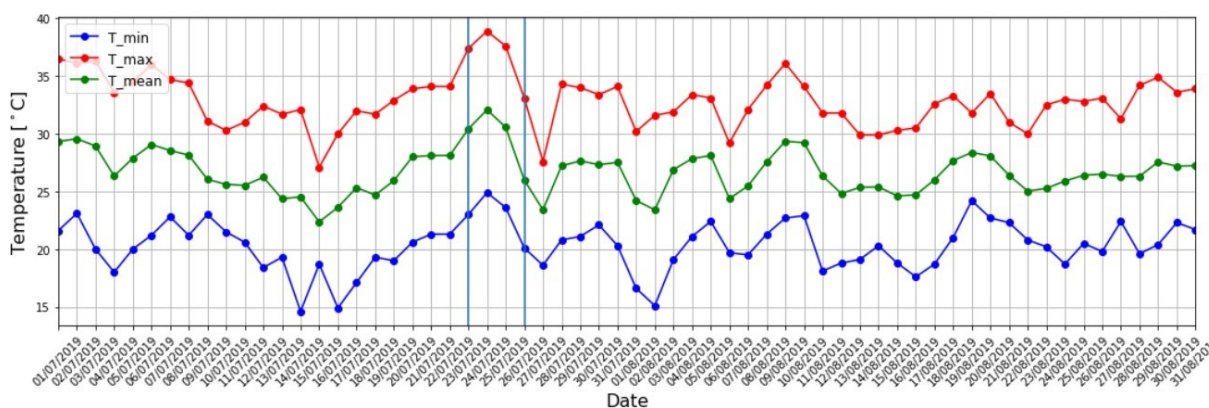


Figure 15. Daily minimum, mean, maximum temperature for the months of July and August 2019. Data come from a weather station located in the urban area of Brescia (see text).

### 3.5.3 UHI formation demonstration

Once temperature data of the two identified weather stations have been obtained, it is possible to make comments about the formation of an UHI in the Ospitaletto territory. Comparing the hourly average of the recorded temperatures for the period January- February 2019 (Figure 16a), it is clear that the UHI is a more evident phenomenon during night hours: it starts at about 12:00 PM and it continues, with a more or less substantial intensity, throughout the night.

During the morning (approximately between 8:00 AM and 12:00 PM), the UHI is less intense, mainly because the surrounding areas are more exposed to solar radiation than the areas within the urban canyon.

In the boxplot in Figure 16c, the hourly differences in temperature (UHI Intensity), between urban and rural meteorological stations, in the winter situation, are shown. Such a graphic representation



confirms the ‘nocturnal’ character of the UHI phenomenon: during the middle hours of the day, which are the hottest, the UHI intensity is close to or lower than zero, while, starting from 3:00 PM, the UHI intensity never drops below the value of 1 °C.

Similarly to the winter situation, also the summer situation has been analysed. Also in this case, observing the behavior of the hourly average of the recorded temperatures for the period July-August 2019 (Figure 16b), one can see that the UHI effect is a phenomenon mainly present during afternoon/night hours. Indeed, only from 11:00 AM the urban temperature becomes higher than the rural one and so it remains overnight, with gradually smaller differences. In the boxplot in Figure 16d, the hourly differences in temperature (UHI Intensity) between urban and rural meteorological stations are shown for the summer situation. The UHI intensity is lower than in the previous case.

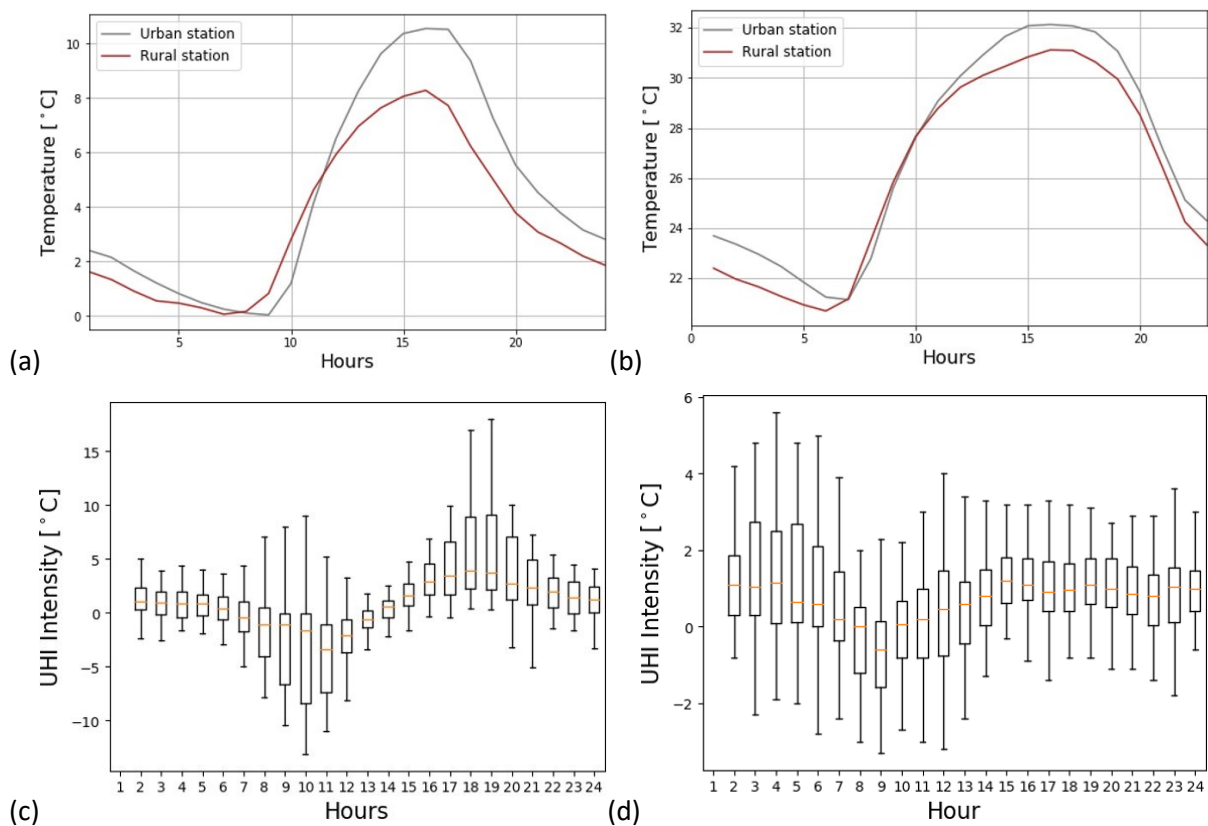


Figure 16. UHI demonstration. Panel (a): recorded temperatures during the months of January-February 2019 from two weather stations, urban (ITAS Pastori station) and rural (Ghedi Airport). Panel (b): recorded temperatures during the months of July-August 2019 from two weather stations, urban and rural. Panel (c): boxplots of hourly temperature differences between ITAS Pastori station and Ghedi Airport station, in the winter season. The bottom and the top of the boxes represent, respectively, the first and the third quartiles (Q1 and Q3), while the line in the middle is the median (Q2). The ends of the whiskers represent, respectively, the lowest datum and the highest datum. Panel (d): boxplots of hourly temperature differences between ITAS Pastori station and Ghedi Airport station in the summer season. Box boundaries are calculated as in panel (c).

### 3.6 Estimation of heating and cooling consumptions

A crucial point of this work is the calculation of the variation of the UHI effect, i.e. the temperature difference between the urban climate and the surrounding areas, due to substitution of a given

amount of conventional heating/cooling equipment with the district heating solutions considered by the LIFE4HeatRecovery project.

In this section, a possible estimation of hourly thermal loads profiles is computed, for both heating and cooling, for both periods of simulation. In order to obtain such hourly time distribution, different steps were taken into account:

- Classification of buildings concerning the territory of Ospitaletto.
- Estimation of the specific energy consumption and extrapolation of a value in terms of kWh/(m<sup>2</sup> y) for each kind of building (i.e., consumption per square meter of building floor area).
- Spatial distribution of consumption, assigning a value in terms of W/m<sup>2</sup> for each cell of the domain (i.e., square meters referred to land area, not floor area).
- Evaluation of a typical hourly profile of consumption, for summer and winter: the daily energy consumption was spread according to the hourly rate.

The estimation of heating and cooling consumption is a key-point for the purpose of this work. Changing them, it will be possible to reproduce the different scenarios of UHI mitigation potential, through waste heat recovery measures, in Ospitaletto. From this, it follows that, inserting the estimation of the consumption related to the cooling of the buildings during the summer period as input for the WRF meteorological model, a scenario that assumes a traditional cooling system will be simulated (it is assumed that the heat released into the atmosphere by cooling systems is not recovered by a 5GDHC network). The same for winter heating: if the estimation of heating consumption is considered as input for the meteorological model, it means that it will be simulated a traditional scenario. On the other hand, simulations that do not foresee, among their inputs, the estimation of energy consumptions related to heating or cooling, correspond to the ideal scenario achievable with the implementation of waste heat recovery measures (as heat is either reused simultaneously or stored in the ground through aquifer wells and not exchanged in the atmosphere). The actual impact of a real 5GDHC network will be in between these two limits.

For this reason, a reliable estimation of building energy consumptions is important in this kind of work, because it allows to characterize the different limiting scenarios. Therefore, special attention was devoted to this point, as explained below.

### 3.6.1 Analysis of the urban context and buildings classification

In order to define thermal load profiles, it is firstly necessary to define and characterize in detail the urban context within which a neutral-temperature DHC network would potentially be applied. The main tool used to carry out this activity was the GIS system of the Lombardy region, in particular related to Ospitaletto municipality; of a such GIS system, the layer "volumetric units" has been used. The main information contained within that layer are presented in Table 2.

Table 2. Description of the main attributes of volumetric units layer.

Attributes	Description
<i>un - vol - qe</i>	Height of the building
<i>SHAPE - Leng</i>	Perimeter of the building
<i>SHAPE - Area</i>	Footprint area of the building

Starting from the information of Table 2 and fixing, according to the iNSPiRe project, an average height of the floors equal to 3 m, it has been possible to compute two important parameters for the buildings classification: the S/V (surface/volume) ratio and the number of floors (estimated from building height assuming a floor height of 3 m), for each building.

Regarding buildings classification, Dipasquale et al., 2014 give information on the heating and cooling demands of residential and office buildings, based on simulations for seven different climate regions covering the whole EU and six different periods of construction (from pre-1945 to post 2000). According to Dipasquale et al., 2019, “the analysis of the European residential building stock allows the individuation of reference buildings that cover around 70% of the entire building stock and whose characteristics follow the ones of the statistics”. Following that project, three main buildings typologies for the residential sectors are therefore individuated: Single Family Houses (SFHs), small Multi-Family Houses (s-MFHs) and large Multi-Family Houses (I-MFHs). The main characteristics of these typologies are summarized in Figure 17.




	SFH	s-MFH	I-MFH
			
<b>Number of storeys</b>	2	3 to 7	3 to 7
<b>Building width/depth</b>	6.5 x 8 m	16.3 x 7.6 m	19.25 x 24 m
<b>Area per storey</b>	50 m <sup>2</sup>	50 m <sup>2</sup>	65 m <sup>2</sup>
<b>S/V ratio</b>	0.90	0.61 to 0.48	0.32 to 0.26
<b>Orientation</b>	45° South-West	45° South-West	45° South-West
<b>Glazing ratio</b>	South 20%; North 10%; East, West 12%	North, South 20%; East & West no windows	North, South 20%; East & West no windows

Figure 17. Reference buildings geometry characteristics (Dipasquale, 2019).

Observing the clusters of buildings in Ospitaletto (from GIS analysis or satellite surveys using Google Earth), it was considered appropriate to identify as representative only buildings with a number of floors lower than 5 (buildings with more than 5 floors, e.g. higher than 15 m, are mostly industrial sheds that do not respect the classification related to residential buildings and are submitted to different classification rules). Not only the number of floors, but also the S/V ratio is a parameter involved in the building classification (Table 3).

Table 3. Buildings classification according to number of floors, S/V ratio and area.

Number of floors	S/V ratio	Area	Class
5	< 0.45	-	I-MFH
4	< 0.45	-	I-MFH
4	> 0.45	-	s-MFH
3	< 0.75	-	s-MFH
2	< 0.75	-	s-MFH
2	> 0.75	-	SFH

1	> 0.75	< 1000 m <sup>2</sup>	SFH
1	> 0.75	> 1000 m <sup>2</sup>	Non-residential

Combining the above classification with Ospitaletto Geoportal data, it was concluded that SFHs cannot have more than 2 floors, MFHs cannot have less than 2 floors and there are no I-MFHs with less than 4 floors. In particular, residential buildings with 5 floors (95%) have a S/V ratio lower than 0.45, i.e. in the typical range of I-MFHs. Hence, a good approximation is to consider all the residential buildings with 5 floors as I-MFHs. The same consideration has been made for residential building with 3 floors: almost 96% of the buildings with 3 floors have a S/V ratio typical of s-MFHs (higher than 0.45, but lower than 0.75), so a good approximation is to consider all the residential buildings with 3 floors as s-MFHs.

For buildings with a number of floors equal to 2 and 4 the approach was the same, but it was not possible to approximate and to establish a unique and defined class for each number of floors: on the one hand, for residential buildings with a number of floors equal to 4, 66% have an S/V ratio typical of s-MFHs (> 0.45), while 34% have an S/V ratio typical of I-MFHs (< 0.45); instead, on the other hand, about 65% of residential buildings with number of floors equal to 2, have an S/V ratio typical of s-MFHs (< 0.75), while 35% have an S/V ratio typical of SFHs (> 0.75).

Buildings with a number of floors equal to 1 need further classification. Ospitaletto is placed in a quite industrialized context: volumetric units with a number of floors equal to 1 are not all residential buildings, but also industrial plants. After checking on Google Earth, a good parameter to distinguish between the two categories turned out to be the footprint area: volumetric units with a footprint area lower than 1000 m<sup>2</sup> are approximately residential buildings (SFHs, according to the previous classification), while volumetric units with a footprint area higher than 1000 m<sup>2</sup> are not residential buildings (schools, factories, sheds). The number of buildings not complying with this classification is very small: there are some non-residential buildings with many floors (some tower), but the overall floor area of these non-classified buildings is about 0.04% of the total floor area in Ospitaletto.

In order to get an idea of the presence of each building category in the municipality of Ospitaletto, in Table 4 the percentage of land covered (m<sup>2</sup>) with respect to the total built-up area (m<sup>2</sup>) is shown.

Table 4. Percentage of land covered for each type of buildings.

Type of building	% land cover
SFHs	0.15
s-MFHs	0.4
I-MFHs	0.02
Non-residential	0.43

As shown in this table, the non-residential area is an important part in the context of Ospitaletto (43%). In such analysis, involving a whole municipal territory, it has been difficult to get a further sub-classification for non-residential buildings. Instead, among residential buildings, s-MFHs are the most widespread (40%), in line with the urban land-use characteristics of Ospitaletto, obtained from the WUDAPT process: in fact, according to the WUDAPT classification, the most common classes in the case study are LCZ 3 and LCZ 6, i.e. those representative of “compact/open mix of low-rise buildings” (1-3 floors).

### 3.6.2 Definition of specific consumption

This estimation was partly based on building simulations and partly on the outcomes of the iNSPiRe and Hotmaps projects.

The starting points are reference buildings modelled by EURAC with the TRNSYS software. Being the most common building type in Ospitaletto, a residential s-MFH with 3 floors was targeted. Other general geometric characteristics were chosen according to the parameters shown in Figure 17.

The specific **space heating** value resulted to be 112.6 kWh/(m<sup>2</sup>·y). This value was then adjusted for the cases of SFH and I-MFH buildings. Here the data of the iNSPiRe project were used (see Deliverable D2.1c, "Simulation results of reference buildings", Chiara Dipasquale and Roberto Fedrizzi, 2014). Here, the effects of various parameters (e.g., internal set point temperature, climatic region, period of construction) were extensively mapped. Applying these procedures, two rescaling factors were identified:

- Ratio of I-MFH to s-MFH specific consumptions: 0.67.
- Ratio of SFH to s-MFH specific consumptions: 1.67.

Large MFH and SFH buildings have respectively smaller and larger specific consumptions than small MFH buildings mainly due to the different surface-volume ratios.

For the non-residential sector it was not possible to rely on simulations. Non-residential buildings have a significant variability and it is was not possible to exploit a simple classification. Therefore, the Hotmaps project toolbox (<https://www.hotmaps.eu/map>) was used instead. This tool provides the overall demand on hectare-size cells (i.e., 100 m × 100 m). Mapping the Ospitaletto area and comparing with the floor area of non-residential buildings, a value of 48.0 kWh/(m<sup>2</sup> y) was estimated for specific heating consumptions.

In conclusion, the space heating consumptions reported in Table 5 were identified.

A similar analysis can be carried out for **specific space cooling** consumptions. However, while in the case of space heating it is reasonable to assume that all buildings have such demand, in the case of space cooling one should take into account that not all buildings are endowed with such cooling plants. The estimated reference specific cooling consumption turned out to be 12 kWh/(m<sup>2</sup> y) for s-MFH buildings with 3 floors. According to the data of the iNSPiRe project, the different effects related to cooling with respect to heating imply that the same value holds also for large MFH buildings. For SFH, instead, an increase by a factor 1.125 is expected. Finally, combining iNSPiRe project data (referred to 2010) with the cooling demand increase observed in recent years (about 6.3 %, according to Andreou et al., 2020), the cooled area can be roughly estimated to be about 10 %.

Concerning non-residential buildings, the usage of the Hotmaps tool provided a specific cooling consumption of about 10.9 kWh/(m<sup>2</sup> y).

In conclusion, the space cooling consumptions reported in Table 6 were identified.

Table 5. Specific space heating thermal energy consumption for the considered building classes.

Type of building	Specific heating consumption [kWh/(m <sup>2</sup> y)]
SFHs	148.43
s-MFHs	112.64
I-MFHs	59.55
Non-residential	48.01

Table 6. Specific space cooling thermal energy consumption for the considered building classes.

Type of building	Specific heating consumption [kWh/(m <sup>2</sup> y)]
SFHs	1.43
s-MFHs	1.28
I-MFHs	1.28
Non-residential	10.87

### 3.6.3 Spatial and temporal distributions

The obtained specific consumptions need then to be distributed in space and time.

#### Spatial distribution

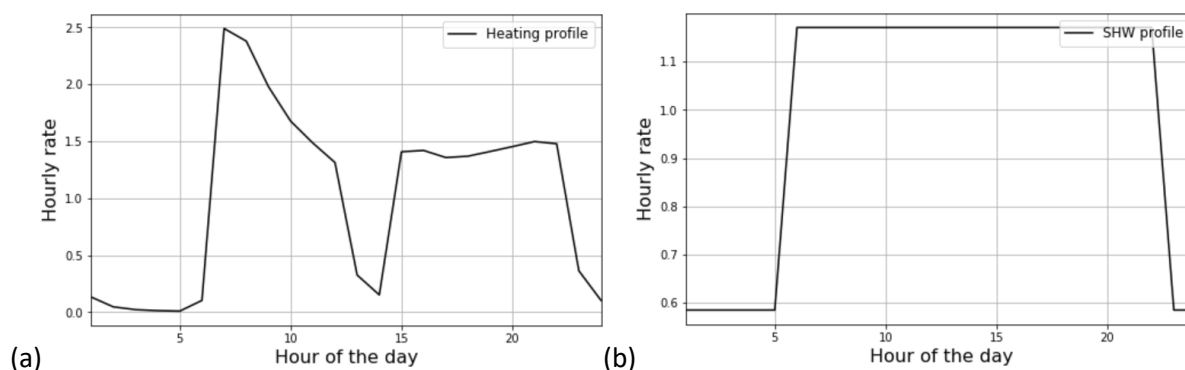
Using QGIS software, for the municipality of Ospitaletto, a grid with 100 m x 100 m of dimension for each cell was created. By assigning the specific heating and cooling consumption values for each kind of building and using QGIS geometric tools to intersect the layer of the buildings (properly including the building height to estimate total floor area and the building type to select the proper specific consumption) with each grid cell, it is possible to obtain the consumption per cell.

#### Temporal distribution

The temporal distribution is necessary to take into account the seasonal variability of the building consumptions. Since the meteorological model simulates the weather conditions on a grid with a side of 300 m x 300 m, the diurnal cycle of energy consumption should refer to a spatial average.

As reference for heating and cooling profiles, simulations performed on EURAC modelled buildings were considered. The profiles for single buildings might exhibit sharp variations, but once the average of multiple buildings is included, some smoothing occurs. To achieve this effect, a 5-hour moving average was applied to single building profiles. Figure 18 in panels a-c shows the steps in creating hourly consumption profiles for heating: (a) individual space heating profile with a morning peak and two main operating cycles, (b) individual sanitary hot water profile with different day-night levels, (c) smoothing through 5-hour moving average on the sum of the two previous profiles.

For cooling, the profile follows approximately the solar cycle, with a slight delay linked to the thermal capacity of buildings (Figure 18d). The peak is at 5:00 PM, but an important increase in consumption occurs already during the morning.



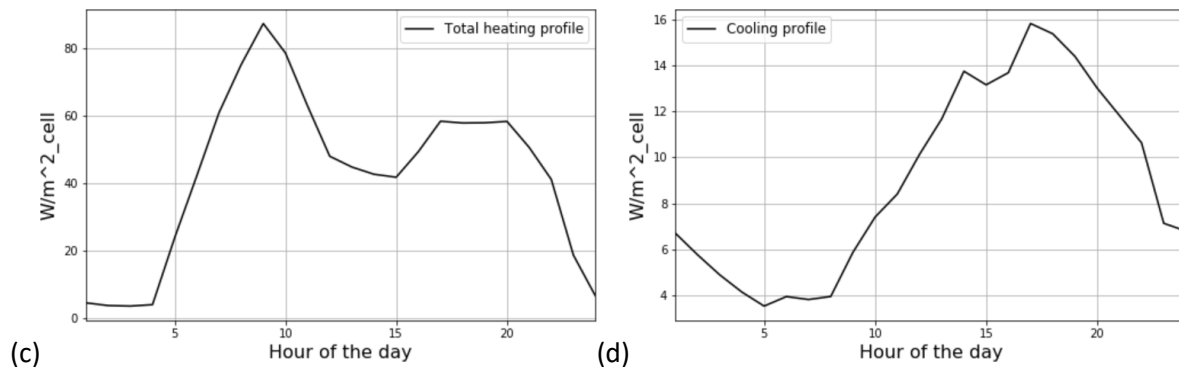


Figure 18. used daily profiles. Panel (a): space heating profile for an individual building. Panel (b): sanitary hot water profile for an individual building, Panel (c): overall smoothed (5-hour moving average) heating profile. Panel (d): cooling profile.

Depending on when anthropogenic heat is released into the atmosphere, the boundary layer situation is different: if the anthropogenic heat is released during night hours, heat emissions tend to heat the urban atmosphere more than day hours, so that the impact on UHI is higher due to the lower mixed layer and more stable atmosphere. During the daytime there is much more mixing effect and the impact of the anthropogenic heat released tends to have a lower impact. Such effect is higher in big cities (Madrid, Hong-Kong, Shanghai, ...), where sensitivity studies show important differences during the daily cycle, while small towns as Ospitaletto react much less to this type of sensitivity analysis.

The last preparation step involves the vector-to-raster tool in QGIS. It allows creating a geo-referenced map, highlighting heating/cooling consumption spatial distribution to be used as input for the simulations. Figure 19 shows the resulting spatial distributions of heating and cooling loads, for the hours with the maximum value. In Ospitaletto's urban context, the heating consumption is higher in the city center than in the suburbs, while, given the current limited uptake of air conditioning systems for residential buildings, the cooling consumption is higher in the industrial zone than in the residential urban area. The highest value for heating load is of about  $60 \text{ W/m}^2$ , while, obviously, for cooling consumption the peak is lower, roughly  $12 \text{ W/m}^2$ .

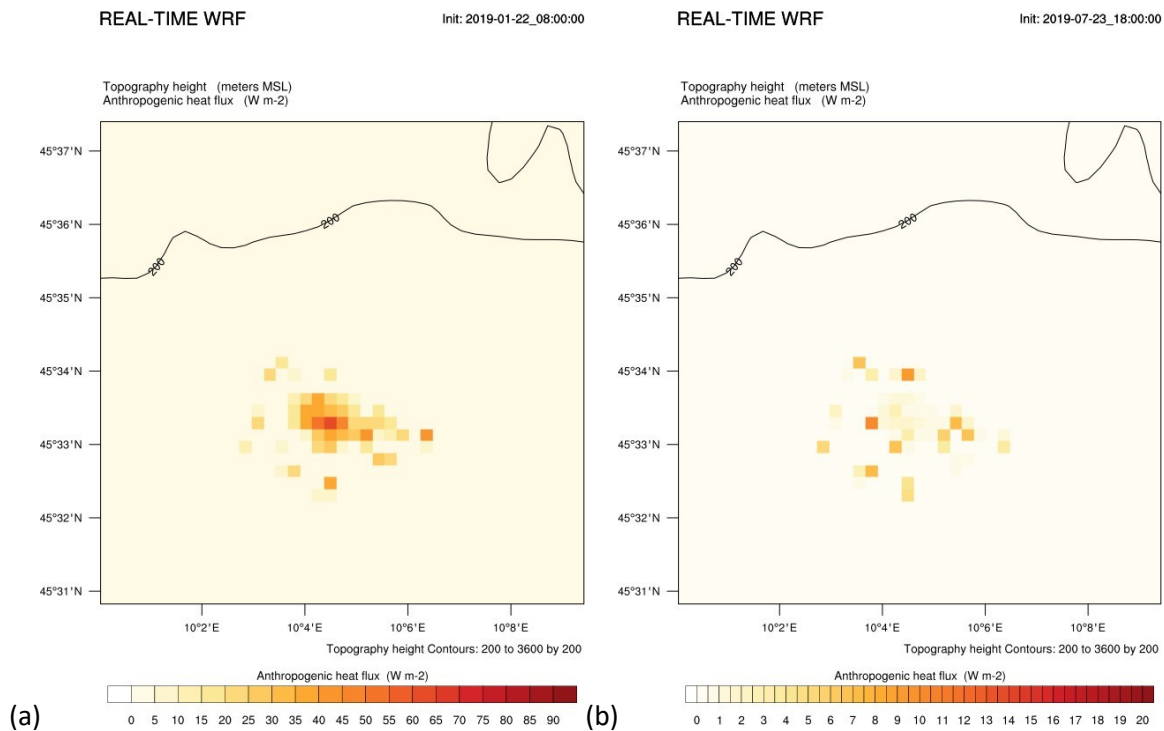


Figure 19. Anthropogenic heat fluxes distribution ( $W/m^2$ ) released by heating and cooling systems. Left panel (a): winter (22 January). Right panel (b): summer (23 July).

## 3.7 Results

This section reports on the obtained simulations results.

### 3.7.1 Simulation model validation

The reliability of the developed model was assessed by comparing the predicted temperature and wind data against measured ones. To this purpose, 11 weather stations located within the region of interested were selected (see Figure 20). The comparison was carried out both for the winter and summer reference days. The quality of the correspondence was measured through the root mean square error (RMSE) and the bias error.

For winter, the comparison was carried out between real data and the scenario including the anthropogenic heat due to heating consumption from conventional systems. This can indeed be considered the case closest to the real situation (the current district heating network in Ospitaletto has a very limited expansion). A similar choice was done for the summer period (i.e., comparison between real data and simulation including the anthropogenic heat due to cooling consumptions assuming a 10 % cooling penetration, see previous section).

As an example, Figure 21 shows the comparison between the hourly measured and simulated temperature data at the locations of the identified weather stations for the winter period Figure 22 and Figure 23 show the corresponding RMSE and relative bias error. Similar plots and results (not reported here) were obtained for wind data and for the summer period as well.

In general, an acceptable agreement was obtained. For example, the statistical parameters of validation RMSE and bias error give values of the order of 2 °C and 1 °C respectively for the winter case.



For the same period, the RMSE and the bias error for wind data was found to be about 1.5 m/s and 1 m/s, respectively (with wind speed ranging from 0 to 6 m/s). Orders of magnitude of errors were in the same range for summer data.



Figure 20. Location of weather meteorological stations within the region of interest.

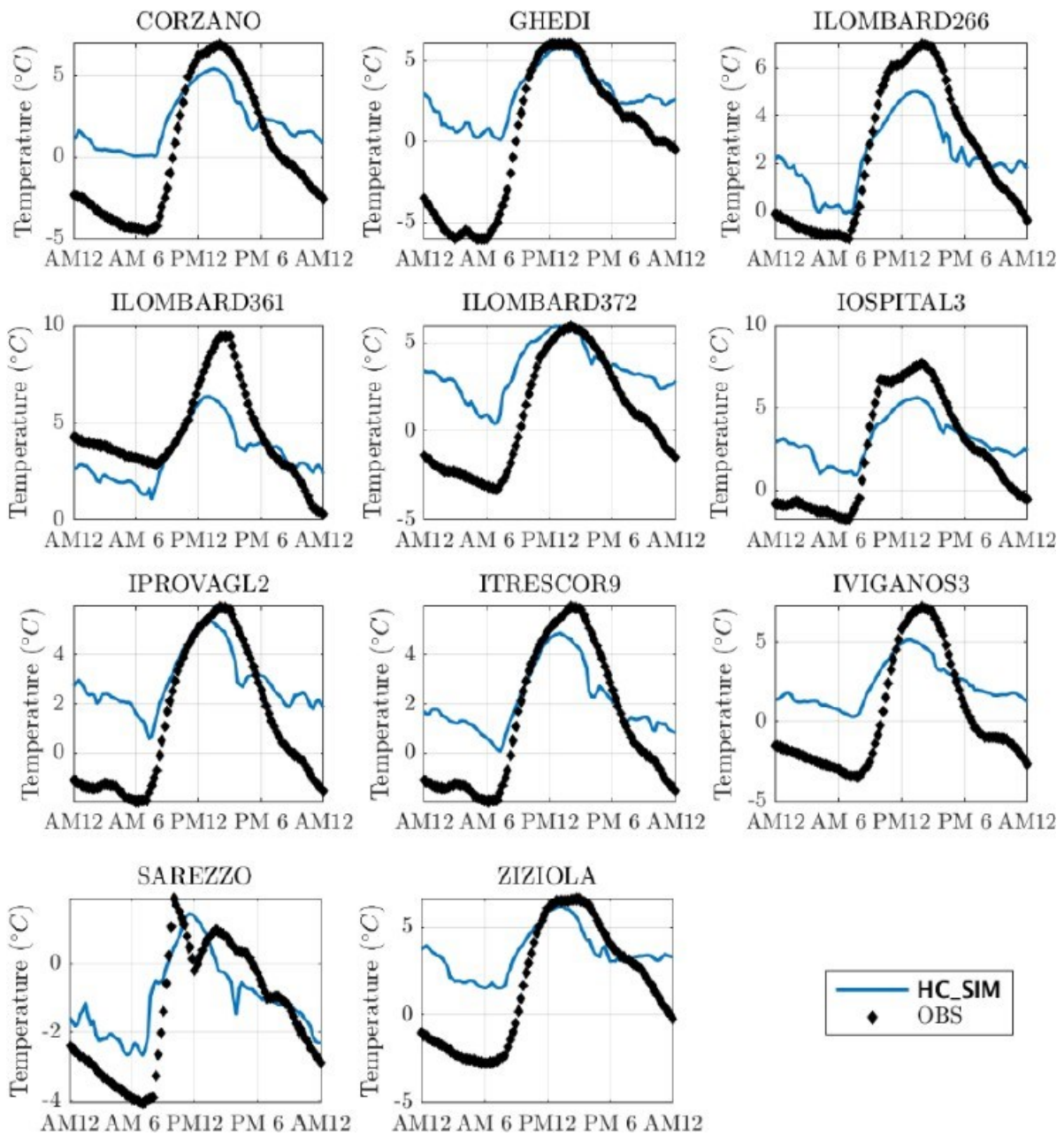


Figure 21. Temperature time series of observational data (black dots) and simulation data (solid blue lines) with heating consumption in winter for the eleven identified meteorological stations.

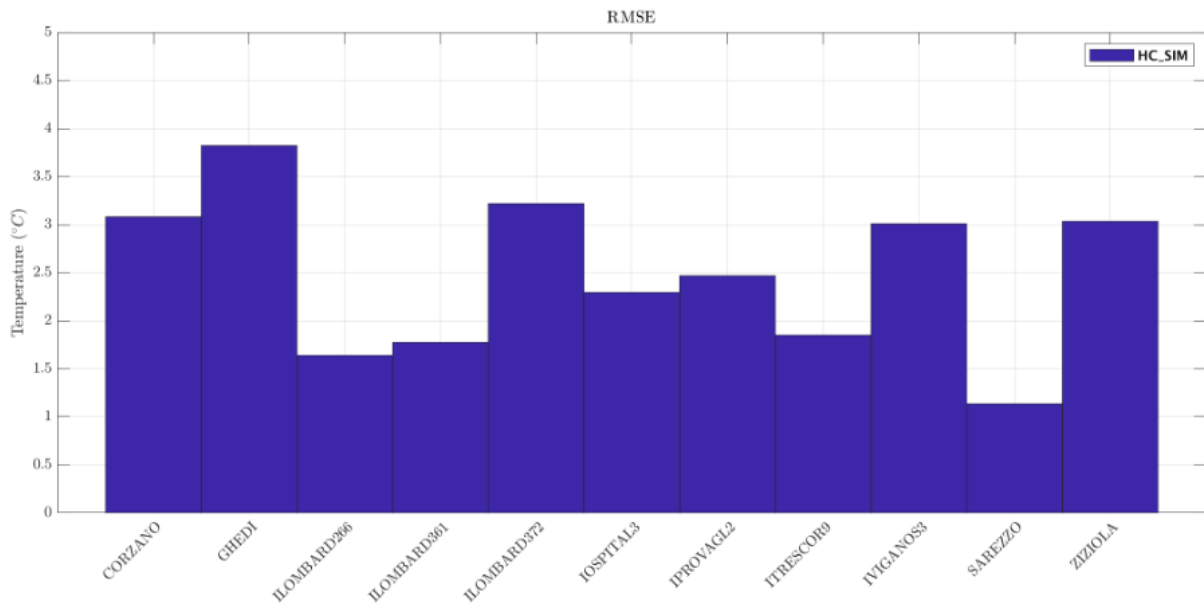


Figure 22. Temperature RMSE in the winter simulation considering anthropogenic heat from heating consumption, for the eleven identified meteorological stations.

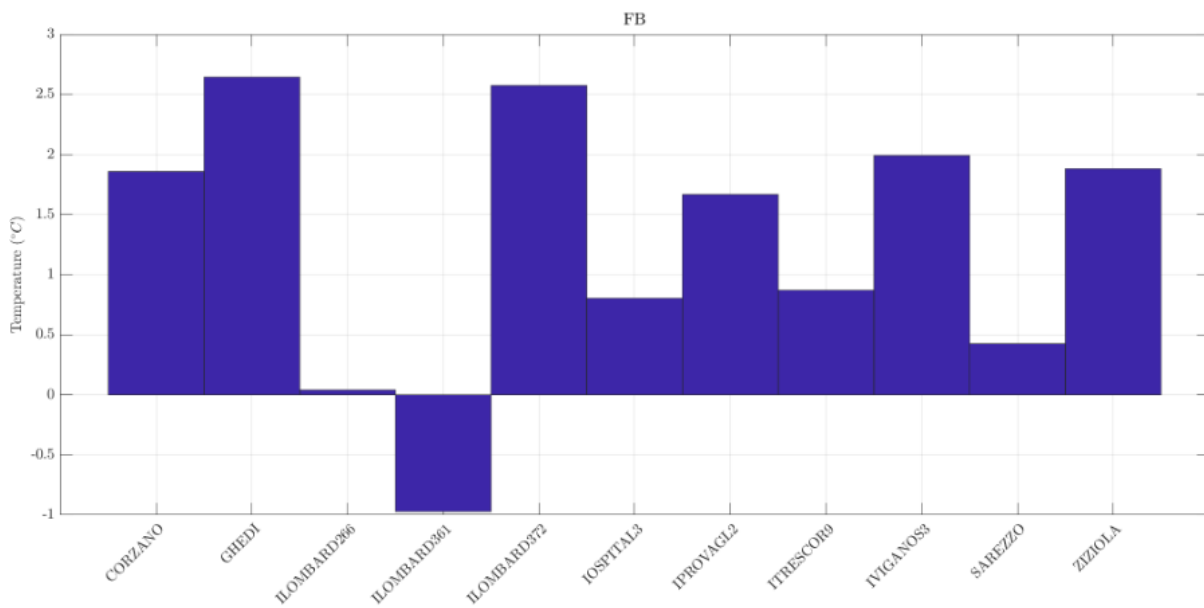


Figure 23. Bias error for temperature in the winter simulation considering anthropogenic heat from heating consumption, for the eleven identified meteorological stations.

### 3.7.2 Temperature and wind maps for the current scenario

In this section, the results of the simulations concerning the winter and summer situations, with and without the contribution of the anthropogenic heat fluxes, are presented. In this work, a period of 36 hours has been simulated for both winter and summer conditions. The first 12 hours are included for initialization purposes, so that the analysis focuses on the following 24 hours (yielding a full winter and a full summer day). Results were obtained for each hour. WRF meteorological model gives hourly outputs referred to UTC time. In reporting outputs, local time has been used.

#### **Winter simulations**

The day identified for the representation of the results for the winter simulation is the 22nd January 2019: it represents one of the coldest days of the winter period, when it is therefore assumed that a substantial use of heating systems will result in important anthropogenic heat fluxes.

Maps of 2-m temperature and 10-m wind vectors for both simulations, one including and one excluding anthropogenic heat from heating consumption were obtained. Results were compared in maps of temperature difference between the two simulations. Moreover, maps of wind speed distribution were recorded. Results were analyzed starting from 4:00 AM to 12:00 AM (six results, every 4 hours). At 4:00 AM, the anthropogenic heat released is very low, but any stirring effect is inhibited: in the urban areas (Ospitaletto city center, the highly industrialized area in the north of Ospitaletto and in the East, where the center of Brescia is located) the temperatures are around 4°C, i.e. higher than the surrounding areas; in the rural areas the temperature is about 2°C. The temperature difference between the two simulations, in Ospitaletto, is negligible, due to the very low heating consumption. At 8:00 AM the anthropogenic heat release is higher (in the simulation in which it is considered) and therefore the temperature difference between the two simulations reaches the value of 0.4°C in the centre of Ospitaletto. The temperature of urban areas is about 3.5°C, while for rural areas it remains around 1°C. The temperature difference between urban and surrounding areas continues to decrease at 12:00 PM. Obviously, the temperature increases during the morning hours and it reaches values of 7°C in the urban areas, but slightly lower in rural areas (5.5°C): the temperature difference between the two simulations, in Ospitaletto, is now 0.3°C. At 4:00 PM and 8:00 PM the situation remains practically the same: the temperature difference between the two simulations is equal to 0.3°C and the temperature difference between urban and rural areas is equal to 1°C and 1.5°C, respectively. Finally, at 12:00 AM, decreasing the temperature difference between the two simulations (around 0.2°C), increases the temperature difference between urban and rural areas (4°C for the urban areas and about 2°C for rural ones). An example of this kind of analysis is visualized in Figure 24, which refers to the time of 4:00 PM, being one with the largest spot differences.

Due to the small size of the town of Ospitaletto, both the UHI effect, which is the temperature difference between urban and rural areas, and the effect of the waste heat release, which is the temperature difference between the simulation considering heating consumption and the one which does not consider it, reach low values.

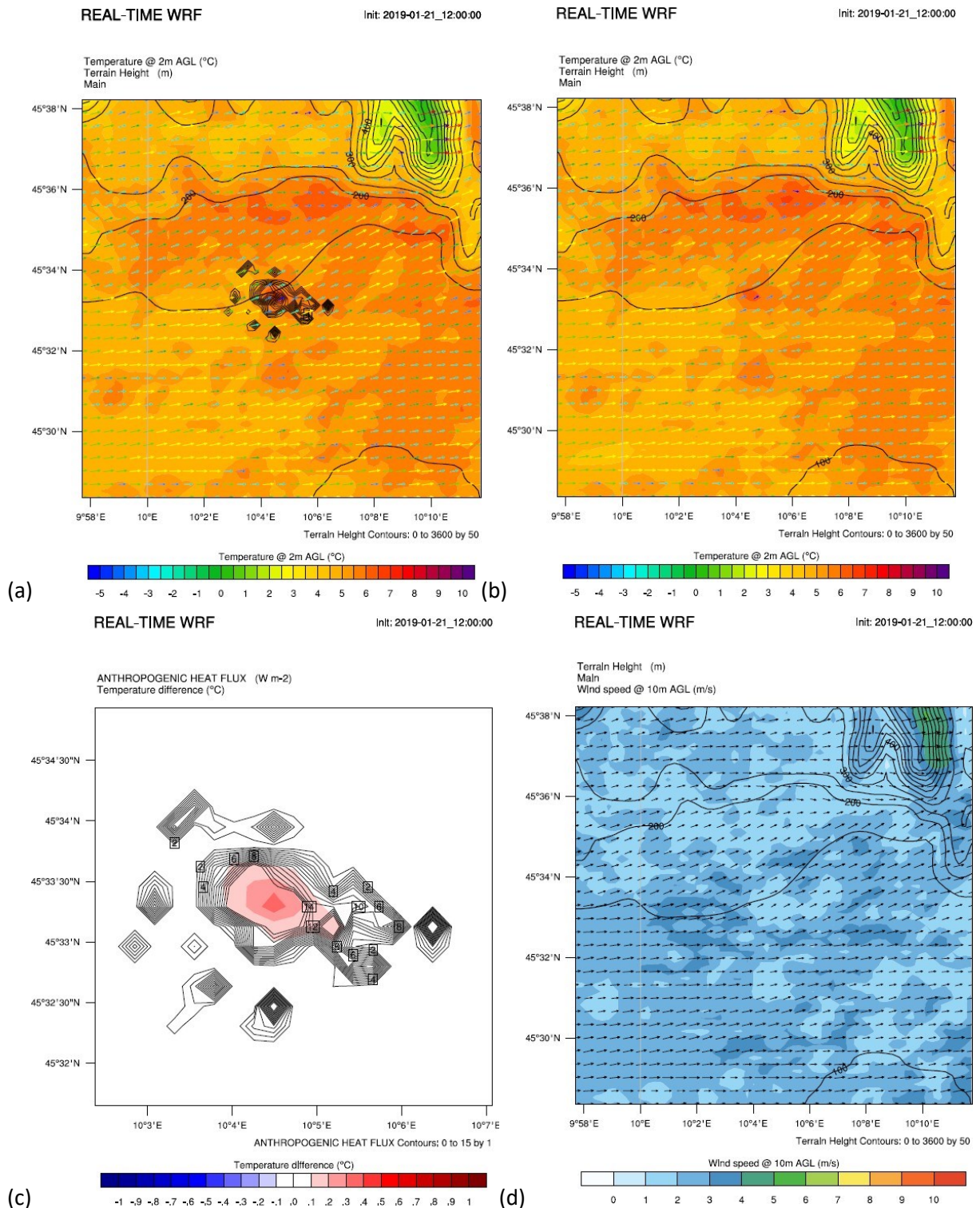


Figure 24. Maps for the simulated winter day at 4:00 PM. Panel (a): map of 2-m air temperature and 10-m wind, considering the presence of anthropogenic heat flux (black lines). Panel (b): same map, in the absence of anthropogenic heat flux. Panel (c): map of 2-m air temperature difference between the two previous simulations. Panel (d): map of 10-m wind speed considering the presence of anthropogenic heat flux (as in panel (a), but including a colour map for wind speed).

The impact of waste heat recovery measures is quantified with a value always lower than 1°C in the city center of Ospitaletto. If, instead of analyzing the difference between the two simulations in a punctual way (as done from above), the average temperature of the urban cells for the two simulations is calculated and the difference along the daily cycle is computed, the behavior of temperature difference along the day is shown in Figure 25. The maximum difference is lower (0.23°C) than the previous representation (0.4°C), but anyway detected in the early hours of the morning and in the late afternoon, as previously seen. The behavior follows approximately the heating consumption daily profile (see previous section).

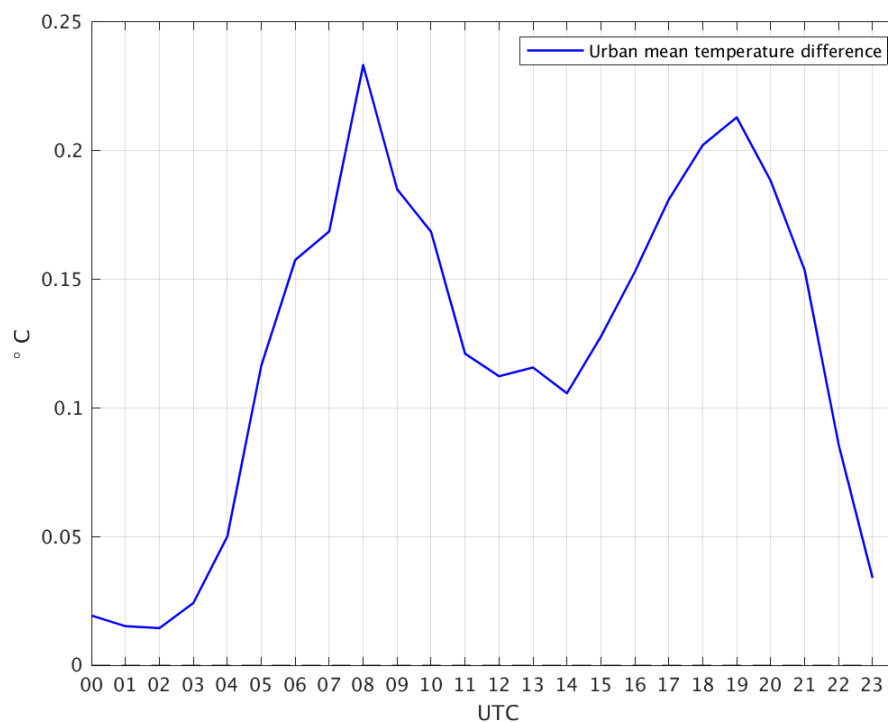


Figure 25. Mean temperature difference, in the urban area of Ospitaletto urban areas, between the two simulations, in the winter scenario, in order to evaluate the impact of heating consumption during the day. UTC time (LST-1) is displayed

In Figure 26, the temperature difference between the central urban cell of Ospitaletto and a representative rural cell, during the full diurnal cycle, is shown. Such analysis refers to the winter simulation considering anthropogenic heat due to heating consumption and allows to quantify the UHI effect occurring in Ospitaletto. The temperature difference between urban and rural zones reaches a maximum value of 3 °C at 5:00 PM with, in general higher values during afternoon and night hours, and lower values during the central hours of the day (1 °C at 1:00 PM). In fact, the average value of the UHI effect is equal to 2.22 °C during the night hours (10:00 PM to 6:00 AM), while it is equal to 1.93 °C during the day hours, confirming the ‘nocturnal’ character of the phenomenon.

As regards the wind, the main direction throughout the day of simulation is W-E (also SW-NE in some moments of the day, especially at 8:00 PM). Analyzing 10-m wind speed from figures like Figure 24, in the urban area of Ospitaletto, the wind intensity never exceeds 2 m/s, with an average value of 1.8 m/s during the day. The wind speed is generally low and is therefore not expected to affect the UHI analysis.

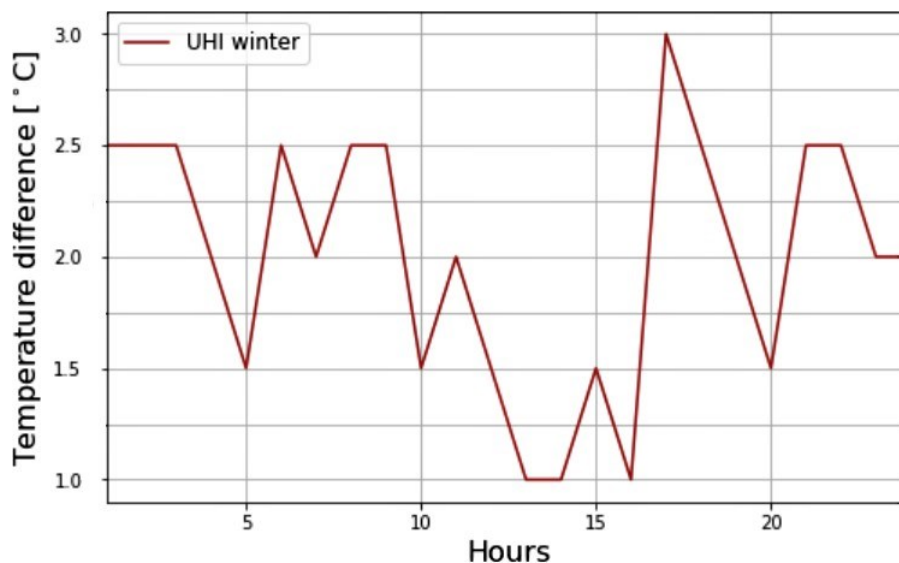


Figure 26. Temperature difference between the central urban cell in Ospitaletto and a representative rural one, in order to evaluate the UHI effect. This analysis refers to the winter simulation, considering heating consumption.

The UHI effect is typically studied in summer, where it increases discomfort for the population. During winter, its presence can instead mitigate the climate and hence reduce heating consumptions with respect to rural areas. The purpose of this analysis is indeed to provide proper boundary conditions for a detailed estimate of the comparative performance of heating solutions. In fact, a solution changing the UHI effect with respect to conventional solutions should be assessed with different (possibly worse, if the UHI effect is reduced) external temperature conditions.

Such results show the nocturnal character of the UHI effect: the temperature differences between urban and rural areas are higher during the afternoon and night hours than at 12:00 PM. In general, the greatest temperature differences between the urban areas and the surrounding areas do not correspond to the moments when a greater release of anthropogenic heat is performed. During the night, the effect of solar radiation, that heats the atmosphere creating convective motions, is absent; even if low values of anthropogenic heat is released during night hours, being the atmospheric boundary layer (the layer within which the air-masses are mixed) very thin, it remains 'trapped' in a layer close to the ground and then it over-heats, in proportion, more than in the day hours. During the day-hours, despite a greater release of anthropogenic heat, the latter is diluted in a thicker atmospheric layer and therefore its effect is not so evident.

Since heating consumptions occur mostly during the day and the UHI effect occurs mostly during the night (being anyway small), the performance of heating systems is not expected to be significantly affected by the latter.

In the map analysis, it was found that unphysical spots in the output of the temperature difference between the two simulations might occur. This effect is the result of numerical errors of the model linked to the convection phenomenon: comparing two different simulations, it could happen that the structures are not exactly overlapped, so the convective bands move from one simulation to another, showing an alternation of light red and blue spots. A possible choice to reduce such undesirable effect of 'spurious convection' is to increase the horizontal coefficient of dispersion. Here, after observing even stronger unphysical effects at lower values, a value of  $K_h = 100 \text{ m}^2/\text{s}$  was chosen. An additional increase was not introduced to avoid other numerical side-effects.

### **Summer simulations**

The day identified for the representation of the results of the summer simulation is 23rd July 2019: it represents one of the hottest days of the summer period, when it is more likely that a substantial use of cooling systems will result in important anthropogenic heat fluxes.

Similar maps as for the winter case were generated, now distinguishing between simulations including and excluding the anthropogenic heat from cooling consumption. Again, simulation results were obtained for every hour and maps were recorded starting from 4:00 AM to 12:00 AM (six results, every 4 hours of the day).

In this section, comments refer to two effects: the temperature difference between the two simulations in the urban area of Ospitaletto and the temperature difference between urban and rural areas (UHI effect).

Concerning the difference between the two simulations, at 4:00 AM, the anthropogenic heat released by cooling systems is very low, so its effect does not generate a temperature increase in urban areas; the same at 8:00 AM. At 12:00 PM an impact of about 0.1°C is reached. At 4:00 PM the difference between the two simulations reaches the highest value of 0.5°C, probably due to 'spurious' numerical errors occurring during the hours of high solar radiation, which generates consistent convective motions. At 8:00 PM, a decrease in the temperature difference between the two simulations towards the value of 0°C is shown. Finally, at 12:00 AM, the temperature difference between the two simulations increases in the western part of the urban area (0.1°C). An example of this kind of analysis is visualized in Figure 27, which refers to the time of 4:00 PM, being one with the largest spot differences.

About the temperature difference between urban and rural areas, at 4:00 AM, in the urban areas the temperatures are around 25.5°C i.e. higher than the rural surrounding areas (23.5°C); at 8:00 AM the temperature of urban areas is about 29.5°C, while for rural areas, about 28.5°C. The temperature difference between urban and surrounding areas, despite low energy consumption values, increases at 12:00 PM due to the consistent solar radiation: the urban temperature reaches values around 36.5°C, while in rural areas it remains equal to 34°C, with a difference of 2.5°C. The UHI effect decreases at 4:00 PM (1.5°C) and at 8:00 PM (1°C). Finally, due to Ospitaletto small dimension and therefore little effect in terms of heat capacity, the temperature difference decreases toward the value of (0.5°C) at 12:00 AM.

The impact of waste heat recovery measures, for the summer scenario, is quantified with a value almost equal to a maximum of 0.1°C in the city center of Ospitaletto.

The mean temperature difference in urban cells, along the day, shows differences lower than 0.1°C (Figure 28). The negative value of 0.04°C at 10:00 PM (UTC) is probably due to numerical errors of the model. The behavior, in this case, does not follow the cooling consumption profile, since values are too low to influence it.



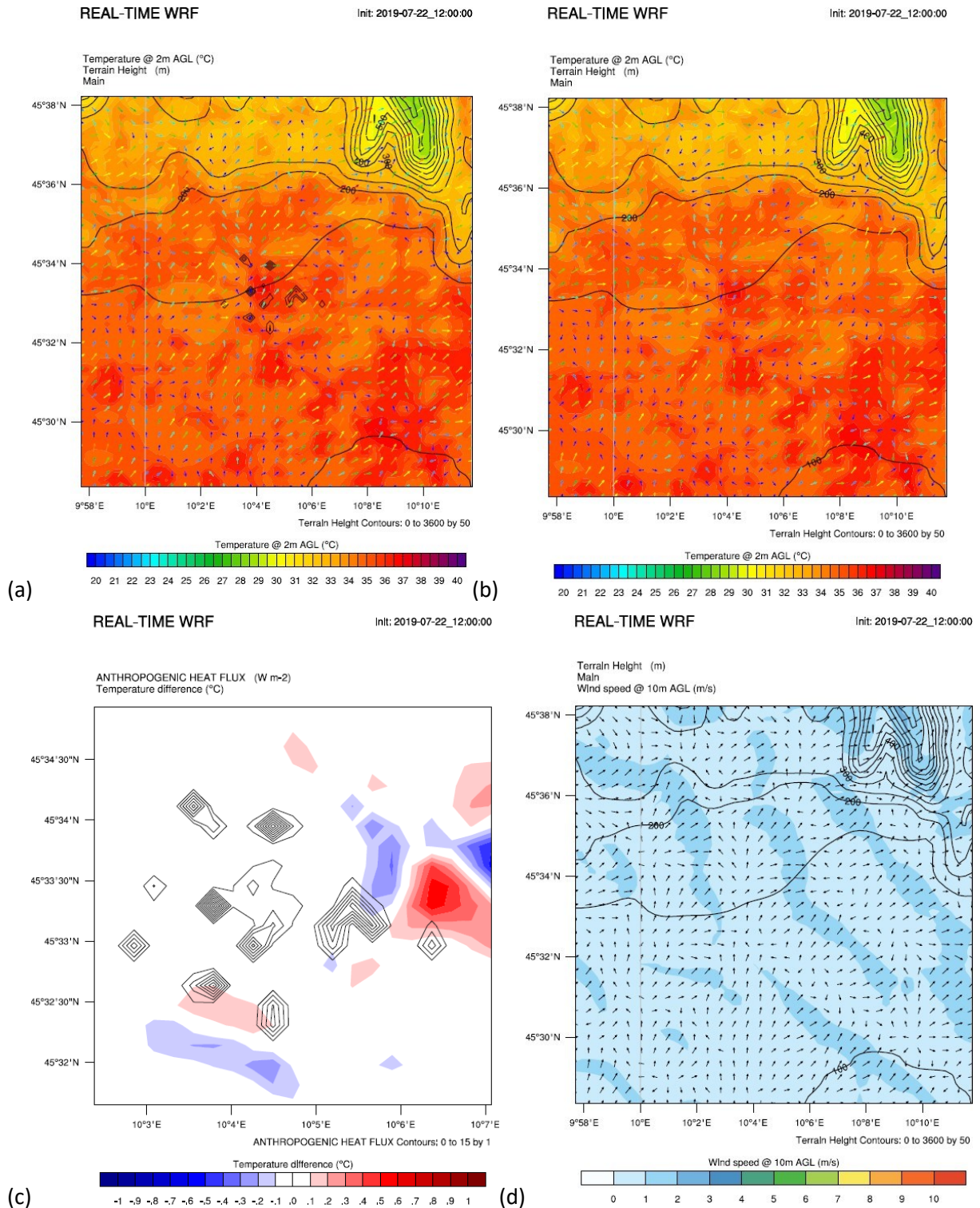


Figure 27. Maps for the simulated summer day at 4:00 PM. Panel (a): map of 2-m air temperature and 10-m wind, considering the presence of anthropogenic heat flux (black lines). Panel (b): same map, in the absence of anthropogenic heat flux. Panel (c): map of 2-m air temperature difference between the two previous simulations. Panel (d): map of 10-m wind speed considering the presence of anthropogenic heat flux (as in panel (a)), but including a colour map for wind speed.

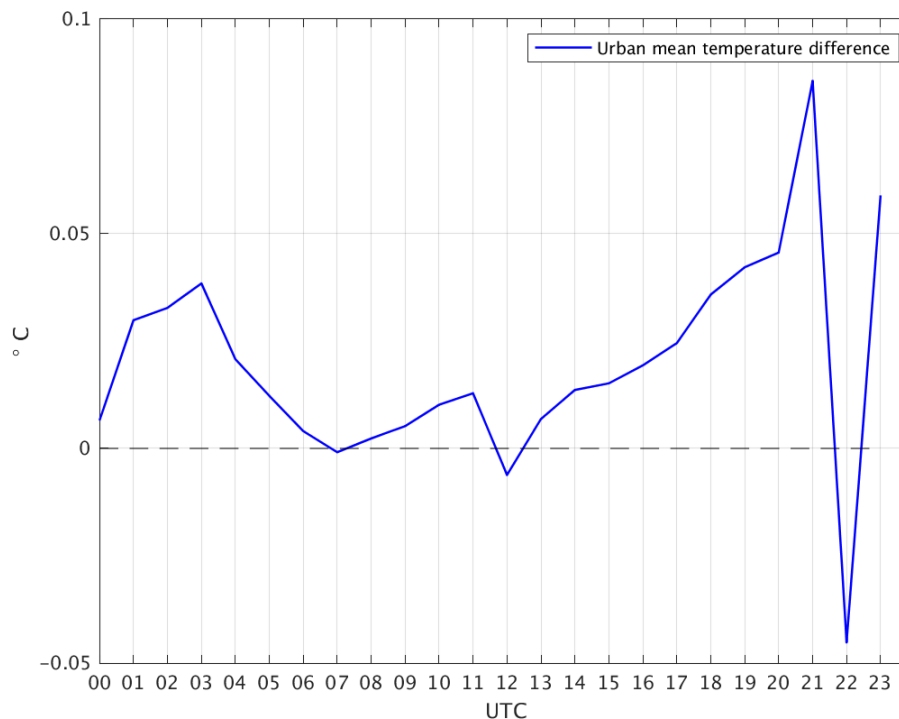


Figure 28. Mean temperature difference, in Ospitaletto urban areas, between the two simulations, in the summer scenario, in order to evaluate the impact of cooling consumption during the day. UTC time (LST-1) is displayed.

Comparing the temperature of the central urban cell of Ospitaletto and a representative rural cell, during the full diurnal cycle, allows quantifying the UHI effect occurring in Ospitaletto. The difference between them is shown in Figure 29, where the simulation which considers anthropogenic heat due to cooling consumption has been analyzed. **Temperature difference between urban and rural zones reaches a maximum value of 2.5°C at 12:00 PM** with, in general, higher values during the central hours of the day, and lower values during afternoon and night hours. The average value of the UHI effect is equal to 1.17°C during the night hours (10:00 PM to 6:00 AM), while it is equal to 1.5°C during the day hours. In this case, the nocturnal character of the UHI is not shown. Two are the main causes: the small size of the urban area of Ospitaletto, which is not able to store heat in building materials, and low values of cooling consumption.

As regards the wind, a main direction it is not evident (as it was in winter): during summer, due to solar radiation, convective motions are generated, an important mixing occurs, showing disordered wind directions, especially in the central hours of the day. Analyzing 10-m simulated wind speed in Ospitaletto's urban area, the wind intensity never exceeds 2 m/s, with an average value of 1.2 m/s during the day. The wind speed is generally low (even less than in the winter scenario) and is therefore not expected to affect the UHI analysis.

Linked to the convective motions, like in the winter situation, undesirable spots in the output of the temperature difference between the two simulations were identified. This effect is again considered to be the result of numerical errors of the model, linked to the convection phenomenon: in order to minimize such 'spurious' errors, it was increased the horizontal coefficient of dispersion ( $K_h = 100 \text{ m}^2/\text{s}$ ) for both simulations.

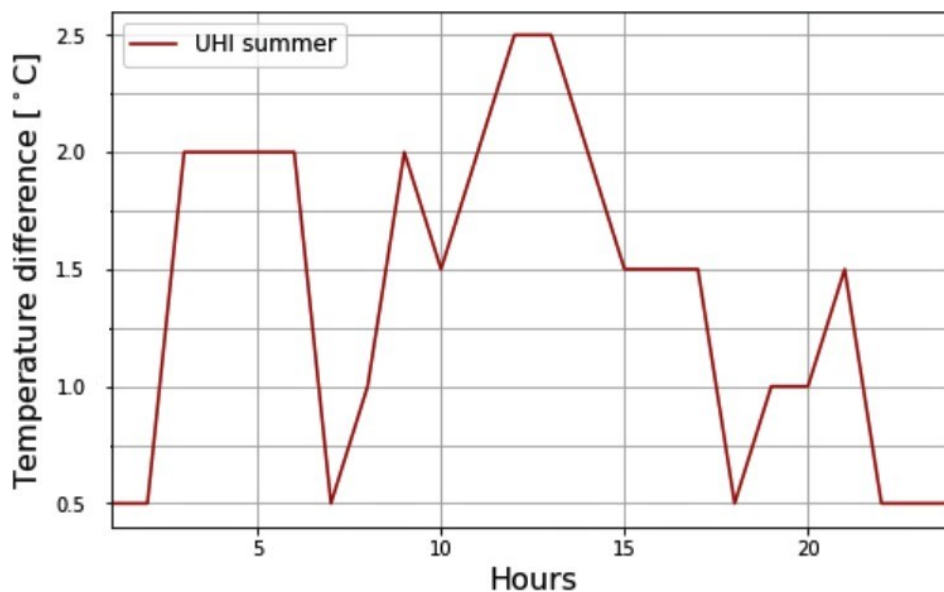


Figure 29. Temperature difference between the central urban cell in Ospitaletto and a representative rural one, in order to evaluate the UHI effect. This analysis refers to summer simulation, considering cooling consumption.

### 3.7.3 Temperature and wind maps for a high-cooling-penetration scenario

The LIFE4HeatRecovery project planned an analysis of the application of low-temperature waste heat recovery measures in the current scenario, but also considering possible future scenarios.

The simulated scenarios in the previous section were related to the analysis of the UHI effect assuming that all the buildings in the context of Ospitaletto are subject to heating of their floor area, but that only 10.6% of the total floor area is cooled (as expected to be in the current situation). In line with the growing trend in the cooling sector, however, it is interesting to consider scenarios with a higher cooling penetration. While separate steps for 2030 and 2050 would be interesting in principle, here simulations were carried out only for the 2050 scenario, since the anthropogenic effect of cooling is low and to observe some differences with respect to 2020, only the highest penetration case was considered.

Thanks to the use of reversible heat pumps installed at the user sites, in the future a neutral-temperature DHC network could be developed, able therefore to satisfy an increasing demand for cooling of the buildings. It is therefore relevant to compare this solution, more environmentally sustainable, with a solution where cooling is all given by individual solutions like split units (no 5GDHC network). In practice, the 5GDHC case is assumed to be equivalent to the absence of anthropogenic heat from cooling (assuming full recycling of heating or storage in the ground), and this is compared with the case of the expected 2050 cooling penetration based on conventional individual chillers.

#### **The chosen 2050 scenario**

The considered scenario only considers an increase in cooling penetration. Otherwise, the inputs of the WRF meteorological model as land-use classification, urban parameters, geographical and meteorological information of the period of simulations remain constant, since in 30 years it is assumed that the structure of the territorial context of Ospitaletto remains almost the same. No global warming forecast is included in the model, focusing only on the assessment of the impact of different technology solutions for cooling under the current boundary conditions. Moreover, only the summer period is considered, as the heating part is not affected by cooling penetration. For simplicity, the 2050

building stock is assumed to be the same as in 2020, also in terms of insulation conditions, though in reality this might improve due to on-going refurbishment. According to the current growth trends, which observe increasing cooling surfaces within urban contexts, what is interesting in this section is the behavior of cooling consumption.

A yearly growth rate for cooling of 10% was assumed (based on observed market trends, Üрге-Vorsatz et al., 2015). Considering, as assumed for the simulation representing the current situation, a current value of 10.6% of cooled area compared to the total area, an increase of 10% per year over 10 years would result in  $10.6\% \times 1.1^{10} = 27.6\%$  of final cooling. This could be a reasonable increase from 2020 to 2030, along an exponential curve. Quick estimates were carried out to assess that under this increase, no significant change in the UHI effect simulations would occur.

It is reasonable to expect that the exponential growth would at some point slow down, possibly settling to a linear growth (Santamouris, 2016). Starting from a value of 10.6% in 2020, the cooled area was estimated to reach 27.6% in 2030 assuming an exponential growth. If linearized, such exponential growth would correspond to about 1.7% of new cooling area per year. As a tentative assumption, this value was then used to roughly estimate the following linear growth phase, which would lead to an additional 34% in 20 years. Considering the uncertainty of this calculation, for simplicity, **the percentage of cooling area was rounded to 50% for the chosen 2050 scenario**. Residential cooling specific consumption values were adjusted accordingly to run new simulations (while non-residential cooling consumptions, estimated from the Hotmaps tool, were assumed to remain unaltered). Spatial and temporal profiles were built as for the current scenario.

Table 7. Specific cooling consumption values for residential buildings in the chosen 2050 scenario.

Type of building	Specific cooling consumption [kWh/(m <sup>2</sup> y)]
SFH	6.75
s-MFH	6.00
I-MFH	6.00

Figure 30 shows the resulting distribution of anthropogenic heat fluxes (W/m<sup>2</sup>). Compared to the distribution obtained for the current scenario, the peak of the spatial distribution of cooling consumption moderately increases up to a value of about 14 W/m<sup>2</sup> for the cell characterized by the maximum value, at the time of maximum consumption, i.e., 6:00 PM (in the current scenario, the consumption peak was around 12 W/m<sup>2</sup>). The peak of the spatial distribution does not change due to the fact that it is related to a cell mostly including industrial cooling (specific cooling consumption for non-residential buildings remains equal to 10.87 kWh/(m<sup>2</sup>·y) for both scenarios). The substantial difference lies instead in the higher average value of the spatial distribution than in the current scenario (average among different cells). Indeed, cells only including residential cooling now have a significantly higher load: especially in the center of Ospitaletto, where the presence of residential buildings is substantial, higher values of anthropogenic heat fluxes than in the previous case are detected.

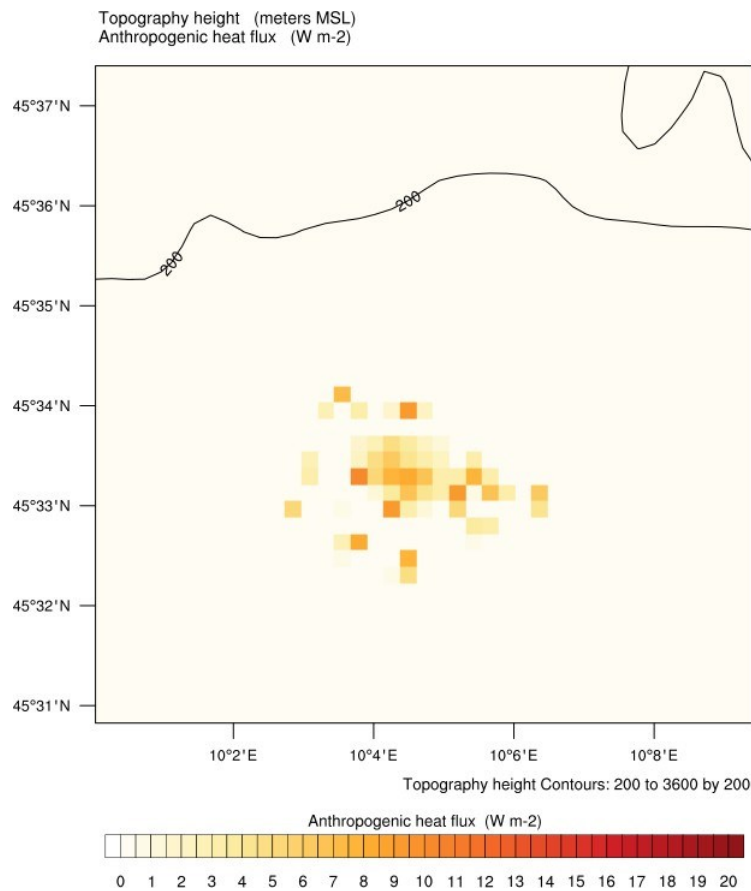


Figure 30. Distribution of anthropogenic heat released by cooling systems in the chosen 2050 scenario.

### Simulation results

As for the current case scenario, a period of 36 hours was simulated, with the first 12 hours included for initialization purposes, so that the analysis focuses on the following 24 hours. The day identified for the analysis corresponds to the boundary conditions of 23rd July 2019 (the same analyzed for the current scenario) because it is assumed that even in the future it could remain one of the hottest days of the summer period, when it is more likely that a substantial use of cooling systems will result in important anthropogenic heat fluxes.

Two effects deserve to be commented: the temperature difference between the two simulations in Ospitaletto urban areas and the temperature difference between urban and rural areas (UHI effect).

Concerning the difference between the simulation with and without anthropogenic heat (the latter being the same carried out for the current scenario), at 4:00 AM, the anthropogenic heat released by the cooling systems is low, so its effect does not generate a temperature increase in urban areas; the same happens at 8:00 AM. At 12:00 PM an impact of about 0.1°C is reached in the urban area of Ospitaletto (higher values appear in anthropized areas North of Ospitaletto, hence not related to the considered cooling penetration). At 4:00 PM the difference between the two simulations reaches the highest value of 0.4°C. Here, however, the same 'spurious' numerical errors occurring in the current summer scenario (linked to consistent convective motions) might affect the result. At 8:00 PM, a

decrease in temperature difference between the two simulations towards the value of 0.1°C is shown. Finally, at 12:00 AM the temperature difference between the two simulations remains, in a small area, equal to (0.1°C). Detecting the outputs for each hour of the day and excluding spurious effects, **the greatest temperature difference between the two simulations is 0.2°C, reached at 5:00 PM**. The maps for 4:00 PM are shown in Figure 31.

Regarding the temperature difference between urban and rural areas, in the 2050 summer simulation considering cooling consumption, at 4:00 AM, in the urban areas the temperatures are around 25.5°C, i.e. higher than the rural surrounding areas (23.5°C); at 8:00 AM the temperature of urban areas is about 29.5°C, while, for rural areas, about 28.5°C. The temperature difference between urban and surrounding areas increases at 12:00 PM: the urban temperature reaches the values of 36°C, while in rural areas it remains equal to 34°C, with a difference of 2°C. The UHI effect decreases at 4:00 PM (1°C) and at 8:00 PM (1°C). Finally, the temperature difference remains equal to (1°C), at 12:00 AM.

The impact of waste heat recovery measures, for the summer scenario, is quantified with a value of about 0.2 °C in the city center of Ospitaletto. Computing the mean temperature of the urban cells for the two simulations and making the difference along the daily cycle, the temperature difference behavior during the day is shown in Figure 32. The maximum difference is lower (0.11°C) than the previous analysis (0.2°C), but anyway visible in the late afternoon. The behavior follows approximately the diurnal cycle, with a slight delay.

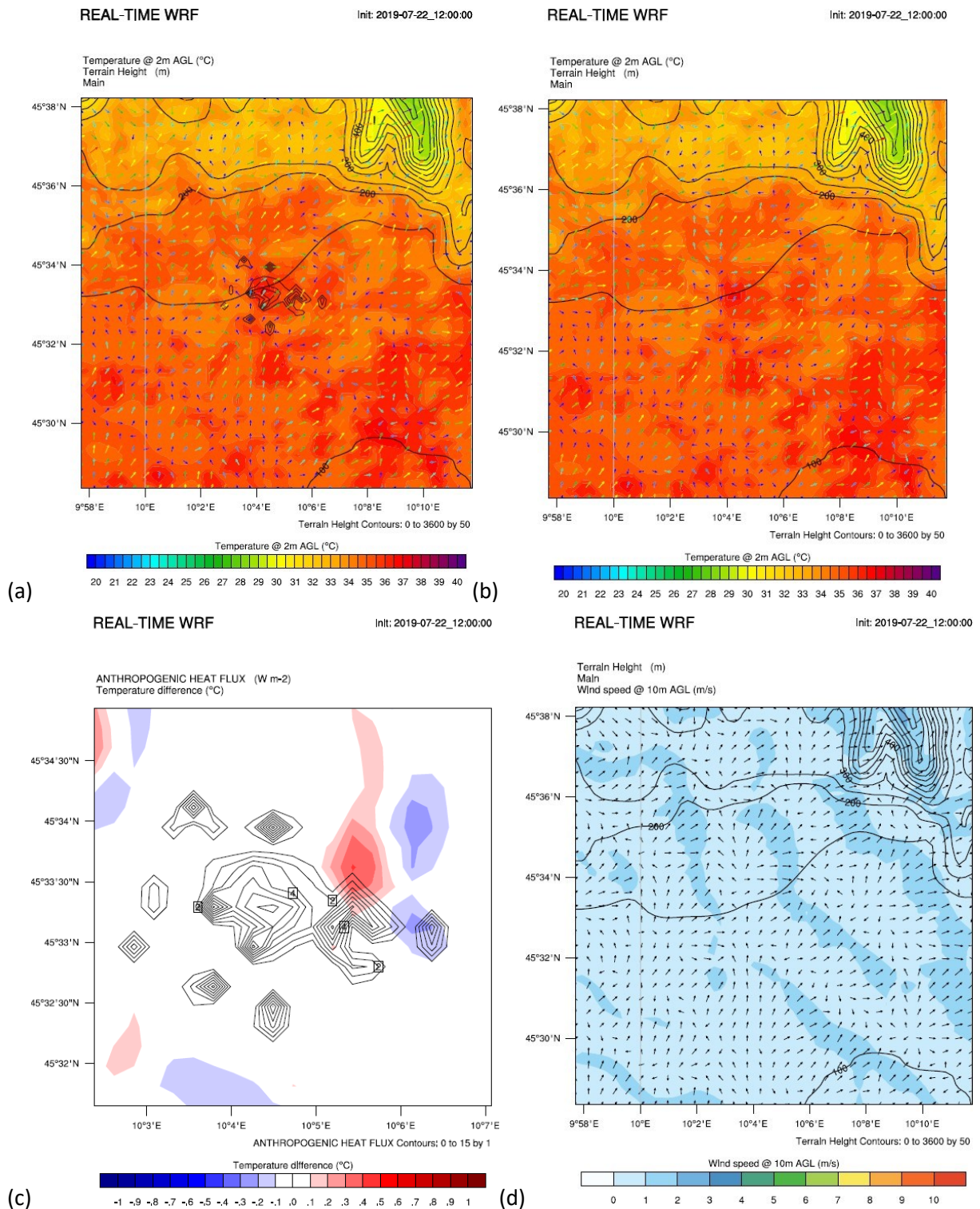


Figure 31. Maps for the simulated summer day at 4:00 PM for the 2050 scenario. Panel (a): map of 2-m air temperature and 10-m wind, considering the presence of anthropogenic heat flux (black lines). Panel (b): same map, in the absence of anthropogenic heat flux. Panel (c): map of 2-m air temperature difference between the two previous simulations. Panel (d): map of 10-m wind speed considering the presence of anthropogenic heat flux (as in panel (a)), but including a colour map for wind

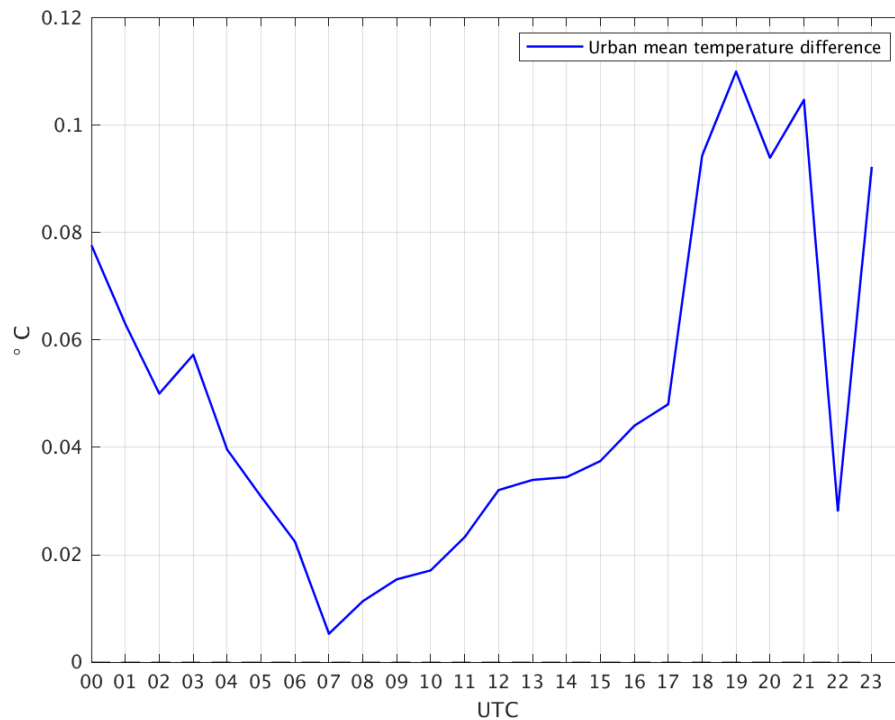


Figure 32. Mean temperature difference, in the urban area of Ospitaletto, between the two simulations, in the 2050 summer scenario, in order to evaluate the impact of cooling consumption during the day. UTC time (LST-1) is displayed.

The comparison between the temperature of the central urban cell of Ospitaletto and a representative rural cell, during the 24 hours of a day, allows quantifying the UHI effect occurring in Ospitaletto, in the 2050 scenario. The difference between them, during the day, is shown in Figure 33, where the simulation which considers anthropogenic heat due to cooling consumption, in the 2050 scenario, was analyzed. Temperature difference between urban and rural zones reaches a maximum value of 2.5°C during night, while lower values in the morning and in the afternoon. The average value of the UHI effect is equal to 1.39°C during the night hours (10:00 PM to 6:00 AM), while equal to 1.3°C during the day hours.

Comparing the results obtained by summer simulations in current scenario and summer simulations in the forecast scenario 2050, two main comments can be made. First, increasing the consumption related to air conditioning, the incidence on the UHI phenomenon moderately increases (0.2°C in the late afternoon) and it remains visible also in the evening: the effect is extended in time, since during afternoon and night hours, an incidence of 0.1°C-0.2°C remains.

The other key point from the comparison between the two summer scenarios is the 'nocturnal' character of the UHI. In the current scenario, due to the low cooling consumption values and the small dimension of Ospitaletto, the city does not retain much heat, showing a low UHI effect during night hours. In the 2050 scenario, with a slightly greater cooling consumption distribution, the heat storage within the buildings materials slightly increases, leading to a corresponding higher temperature difference between urban and rural areas, during night hours. However, due to the small differences, comparable with the simulation error, it cannot be quantitatively concluded that this behavior should be attributed to the increased cooling only.



As regards the wind, a main direction it is not evident (as in previous summer case). Analyzing 10-m wind speed, the wind intensity never exceeds 2 m/s, with an average value of 1.4 m/s during the day. Also in this scenario, the wind speed is generally low and is therefore not expected to affect the UHI analysis.

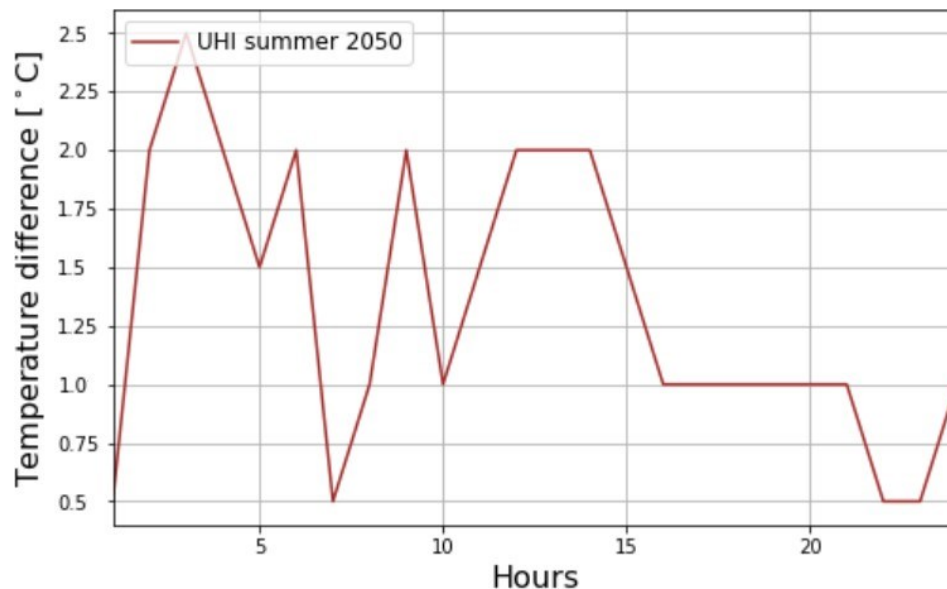


Figure 33. Temperature difference between the central urban cell in Ospitaletto and a representative rural one, in order to evaluate the UHI effect. This analysis refers to summer simulation, considering cooling consumptions for the the 2050 scenario.

### 3.7.4 Result interpretation and summary of Ospitaletto analysis

It is useful to review the interpretation of the anthropogenic heat flux, in both winter and summer seasons.

In winter, the anthropogenic heat flux is due to heating: every building, in the current situation, typically has a gas boiler that releases heat into the atmosphere and therefore it generates heat locally. With a neutral-temperature DH, buildings are still heated, but a different source is used and heat, which would otherwise be dispersed as waste heat, is recirculated: the heat released is no longer produced in the residential area (burning gas in the boiler), but it is produced by recycled waste heat elsewhere. By replacing the gas boiler with a 5GDHC network, the building continues to be heated and such heat is still transmitted into the atmosphere, but in lower quantities (part of the heat is recycled).

Focusing on the case of Ospitaletto, without neutral-temperature DH, the heat produced by residential heating and industrial activities in the territory is released into the atmosphere. By introducing the 5GDHC network and, in particular applications like the LIFE4HeatRecovery demo in Ospitaletto (waste heat recovery from a steel manufacturing company), the waste heat is no longer released into the atmosphere near the factory, but it is used to meet residential heating demand (from the buildings however it will still be dispersed). The reduction in the emission of anthropogenic heat fluxes takes place in areas where waste heat recovery occurs, while, in the residential zones, the reduction could be not so substantial.

The simulations performed here show the difference between the case with heating and with no heating at all. This is a stronger effect than the one generated by the actual transition from

conventional heating to a neutral-temperature network. It was considered however interesting to analyse this “extreme” case, which can be seen as the theoretical limit where also the heat released by buildings is absent, as if for a perfect insulation. This was useful to enhance the observable changes, in consideration of the low heat fluxes present in the Ospitaletto case.

In summer, the anthropogenic heat flux is given by the heat generated by the bodies of people and by the heat generated by equipment and machines: in the current situation, the most common cooling systems are split units, with the fan inside the house and the condensing part outside the house. Cooling systems work on the principle of refrigeration cycles: the part of energy actually generated inside a refrigerator is only the electrical part, the rest is transferred, i.e. a recirculation occurs; similarly for a building where, due to the not perfect insulation, heat penetrates from the outside and it is expelled from the machine but, to do that, it spends a share of electricity. The recirculated part does not contribute to the “purely” anthropogenic heat flux, but what it is produced by buildings in terms of anthropogenic heat is the heat linked to the bodies of people and the part of electricity consumed by machines.

Introducing a neutral-temperature DHC network, therefore able to work even in cooling mode, differences in respect to the heating scenario occur. In the case of cooling with a neutral-temperature network, heat is removed from buildings, it is sent into the network and pushed away: heat can be trapped in the ground for a long period (seasonal accumulation) or dispersed in an aquifer, in a groundwater or surface water stream, flowing outside the city. Note also that the cooling system not only absorbs purely anthropogenic heat, but also part of the ambient heat entered into buildings due to lack of insulation.

Focusing on 2050 scenario in Ospitaletto, the situation could involve having split units installed in each house, with the corresponding electricity that, in a traditional scenario, goes into the atmosphere. By introducing neutral-temperature DHC network, not only that part of electricity is reduced due to the increase in efficiency of the system, but it is also removed from buildings and sent elsewhere. In such a scenario, the network not only removes the anthropogenic heat related to cooling, but, even more, it removes heat from the urban areas and sends it away. This can be seen as a “negative” anthropogenic effect at local (urban) level (though at global level heat is of course only dispersed somewhere else).

According to this point of view, the cooling demand profiles used in these simulations correspond to the cooling thermal power needed by buildings, not only to the electric part of cooling machines. Hence, the case with cooling consumptions does not exactly represent the case of traditional equipment; similarly, the case without cooling consumptions does not exactly represent the case of cooling with a neutral-temperature network. However, the difference between the two simulated cases is in fact the same as the difference between the two types of cooling solutions, since the neutral-temperature network effectively subtracts the thermal cooling load from the urban area.

Summarizing, this chapter presented the results of winter and summer simulations generated by the meteorological model, which contains a physical parameterization (BEP) able to simulate the effect of urban land-mask on the atmospheric dynamics.

First, the model validation was carried out, based on 11 meteorological stations located in the region of interest. As regards temperature, a better quality of the model is observed in simulating the summer rather than the winter season, while for the wind, the quality of the model is almost similar for both seasonal scenarios. Observed deviations were anyway in an acceptable range. Moreover, in the analysis about differences between simulations, inaccuracies of the same type are expected to be cancelled out.

Afterwards, simulation outputs have been analyzed. A typical day has been considered, analyzing the results every 4 hours, for a total of 6 outputs per day. Both the results for the difference in temperature between the simulation considering anthropogenic fluxes and without considering them and for the difference in temperature between Ospitaletto's urban area and surrounding areas (UHI effect) have been discussed. The results show that, due to Ospitaletto's small dimension, the observed differences in temperature are low. About the wind, for such low wind speed values, the wind impact on the UHI effect is expected to be negligible.

On the other hand, it was observed that there is some relation between the increment in the release of anthropogenic heat and a stronger UHI effect, though it is a weak effect since the physical phenomena that occur in the atmosphere need to be considered: convective motions, that lead to a mixing of air masses, are favored during the middle hours of the day, ensuring greater dispersion of anthropogenic heat at ground level compared to what happens at night, where the atmosphere is more stable and convective motions are almost inhibited. For example, average deviations of only small fractions of degree ( $< 0.1$  °C) can be attributed to anthropogenic heat in summer, under the current cooling consumption situation. Nevertheless, spot differences (still at the level of the considered grid cells, with a 300 m side) can be a few times higher. Higher cooling penetration scenarios contributed to enhancing these effects, though they were found to remain rather small, possibly reaching about 0.5 °C.

## 4 Heerlen case

Heerlen is a city located in the southeast of the Netherlands (50°53'N, 5°59'E), at an elevation of about 113 m. It is part of the province of Limburg. More precisely, it is part of Parkstad Limburg, a city-region agglomerate including other 7 municipalities, Heerlen being one of the largest ones. Heerlen municipality has a population of about 87,000 inhabitants (while the entire Parkstad Limburg has a population of about 250,000 inhabitants).

Heerlen has a distance of about 20 km from Maastricht (the Netherlands, about 120,000 inhabitants), and of about 15 km from Aachen (Germany, about 250,000 inhabitants). Due to the easier availability of temperature data for these cities and their comparable location and size, it was decided to resort to the corresponding measurements for a simplified analysis, see Figure 34.

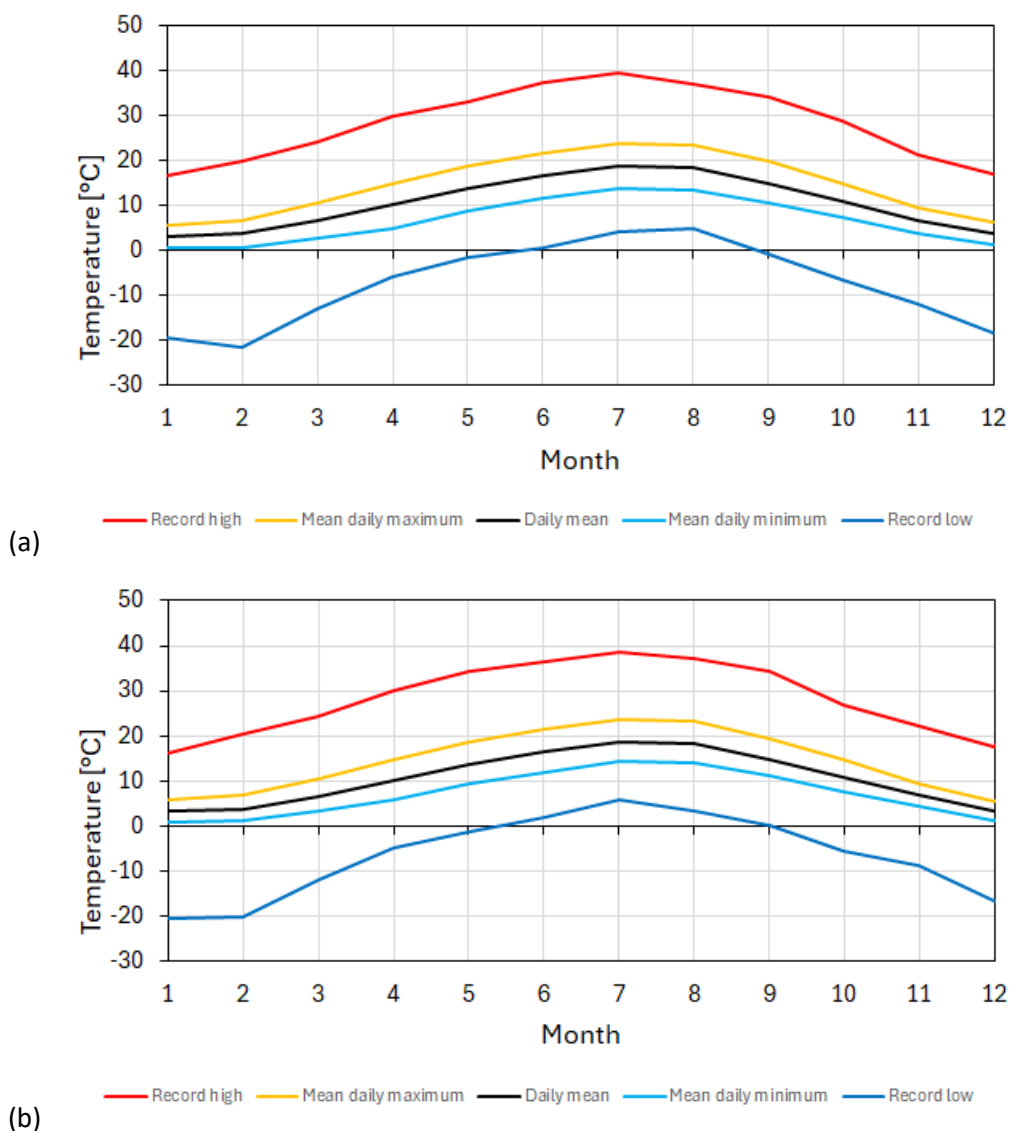


Figure 34. Monthly temperatures for Maastricht (panel (a), top; about 20 km from Heerlen as-the-crow-flies; data taken from the Royal Netherlands Meteorological Institute, 1991-2020 normals) and Aachen (panel (b), bottom; about 15 km from Heerlen as-the-crow-flies; data taken from Deutscher Wetterdienst, 1991-2020 normals).

As it can be seen from Figure 34, the two considered locations have very similar temperatures, in spite of the slightly different size of the cities.

As it can be expected due to the different geographical location, average summer temperatures of this region are a few degrees lower than those observed in Ospitaletto.

To assess the urban heat island effect is concerned, as discussed in the previous chapter, urban temperatures should be compared with rural ones. From this point of view, it should be noted that Aachen, due to the larger city size and due to the surrounding hills, can exhibit stronger urban heat island effects than Maastricht (and even more than Heerlen). It is hence uncertain to which extent data from another city can be extrapolated to a different one. Considering that in all cases a small UHI effect is expected for Heerlen (due to the relatively small city size and the northern temperate climate zone), a slightly different point of view was taken for this analysis.

In particular, 3 Dutch cities were targeted for a simplified analysis, namely Heerlen, Rotterdam, and Amsterdam. The UHI effect was estimated for Rotterdam and Amsterdam, thanks to literature data. The impact of cooling systems was then assessed in a similar way to what discussed for Ospitaletto, based on urban data.

#### 4.1.1 UHI effect in Rotterdam and Amsterdam

For the case of Rotterdam, an assessment of the UHI effect was carried out in 2010 in the report “Ruimtelijke verdeling en mogelijke oorzaken van het hitte-eiland effect” (Spatial distribution and possible causes of the heat island effect), by L. Klok et al. (TNO-034-UT-2010-01229). Here the authors combined different approaches, similarly to what described in the previous chapter. In particular, Figure 35 shows the average surface temperature in summer days (June-August) as retrieved from a collection of 15 Landsat images, ranging from 1984 to 2007 (see the original report for details about the averaging process).

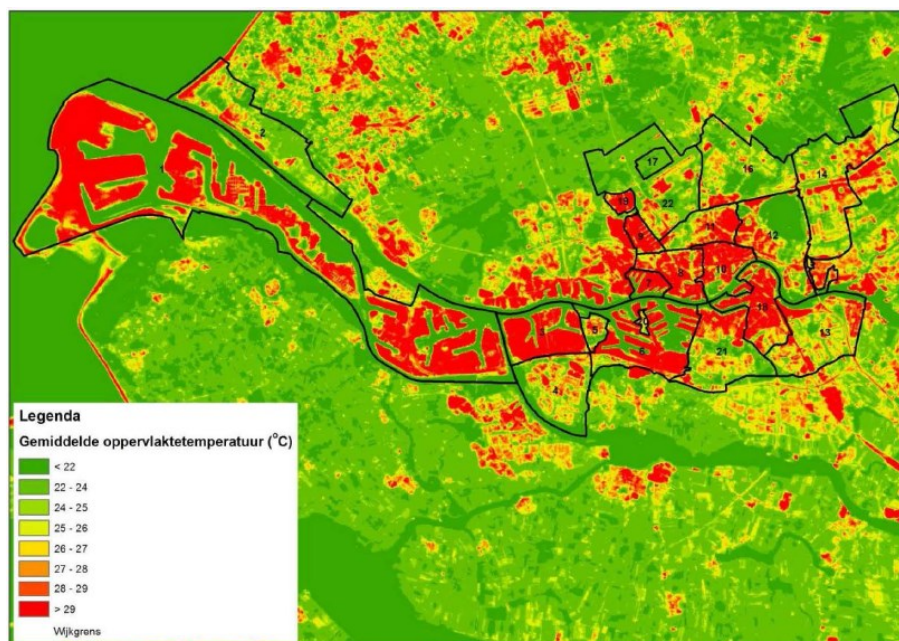


Figure 35. Average daytime surface temperature of Rotterdam based on a collection of 15 Landsat images. Converted to a resolution of 30 m. See text.

It can be seen in Figure 35 that, across the 22 districts of Rotterdam, variations of more than 7 °C occur (note that the Rotterdam area also includes various water channels, all at a temperature of about 22 °C in these periods). A more detailed analysis identified **UHIs with up to 9.9 °C of temperature difference** with respect to the rural area. Cities with water bodies and close to the sea can be subject to stronger urban-rural temperature differences, nevertheless the effect is remarkably high. This also shows how a **local analysis** (more appropriate and feasible for large cities, rather than for small cities like Ospitaletto) can be important to highlight fluctuations much higher than the average.

For the case of Amsterdam (where again the presence of water bodies is significant), for the purpose of this analysis a very simplified approach was adopted, resorting to the website <http://maps.amsterdam.nl>, managed by Amsterdam municipality. Here, various maps are available, including a heat map. A sample image from summer 2024 is shown in Figure 36, showing UHI effects of the **same order of magnitude as for Rotterdam**.

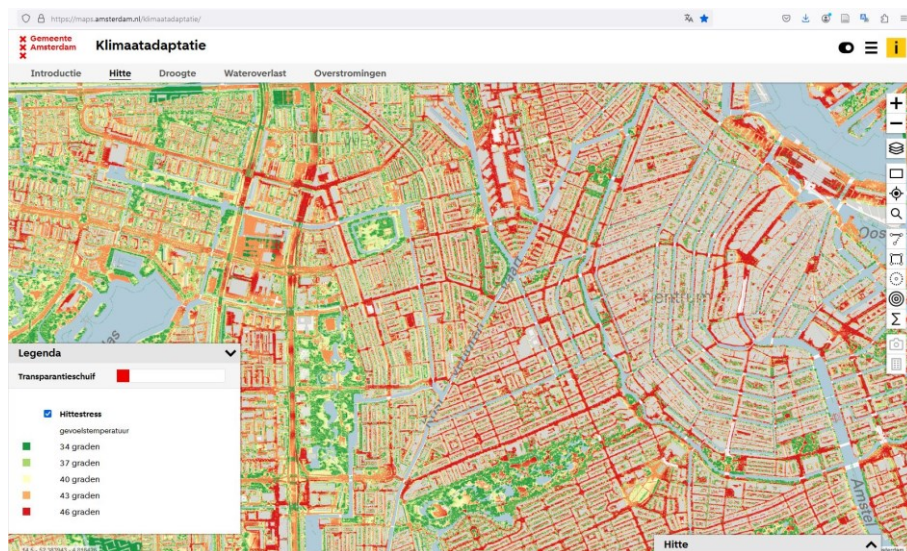


Figure 36. Screenshot from the website <http://maps.amsterdam.nl>, managed by Amsterdam municipality. Local high-temperature fluctuations can be clearly recognized. Even though the measurement uncertainty in these maps can be expected to be significant (a few degrees, hence questioning the accuracy of the shown absolute temperature values), the observed order of magnitude of 10 K difference between min and max temperatures is in line with the results reported for Rotterdam.

#### 4.1.2 Cooling power estimates and urban data for Heerlen, Rotterdam, and Amsterdam

In the previous section, it has been shown the possible high intensity of the UHI effect in large cities, even in relatively northern EU regions like the Netherlands. In terms of anthropogenic heat and mitigation potential, an analysis similar to the one presented for the Ospitaletto case was carried out by Mijwater. The focus was on the cooling effect in summer, where UHIs cause the highest discomfort.

As discussed for Ospitaletto, the actual anthropogenic heat source due by conventional cooling solutions (e.g., split units) is given by the corresponding electricity consumption. On average, this is a negligible effect with respect to other heat sources. On the other hand, this source can be concentrated in small zones and in short periods of the day, where the effect can become significant. Since, similarly to Ospitaletto, the Mijwater system can be classified as a 5GDHC system, it is interesting to discuss its UHI mitigation potential. In practice, while conventional cooling solutions

contribute to net urban heat with their electricity consumptions, 5GDHC networks not only avoid this local electricity-related heat emission, but even absorb the thermal cooling load and reject or store it elsewhere. Hence, 5GDHC networks can remove heat from the urban environment with a potential 3-4 times higher (due to corresponding COP values) than the estimate related to pure anthropogenic heat (i.e., chiller electricity).

Mijnwater carried out an analysis based on different simplified estimation methods, to assess the heat density associated to cooling, measured in  $W/m^2$ . While results were found to vary on a significant range depending on the chosen method, the **orders of magnitude were roughly in agreement with the ones found for Ospitaletto** (the focus was on high cooling penetration scenarios). Moreover, a comparison of the average urban typologies of the considered cities was carried out, yielding the results reported in Table 8.

Table 8. Urban typology (expressed in terms of building density and plot ratio) for the three considered Dutch cities.

City	Dwelling density [1/km <sup>2</sup> ]	Dwelling average floor area [m <sup>2</sup> ]	Plot ratio (m <sup>2</sup> floor area / m <sup>2</sup> land area)
Amsterdam	2615	125	0.33
Heerlen	1018	125	0.13
Rotterdam	1431	125	0.18

Not surprisingly, Heerlen is not only a smaller city than Amsterdam and Rotterdam, but it also has a lower urban density. Consequently, no significant UHI effect is expected for Heerlen. Nevertheless, the present review shows how the UHI effect is far from being negligible also for cities in relatively northern Europe regions like the Netherlands. Moreover, while on average the UHI effect can be rather small, local islands can exhibit significant temperature differences (order of 10 K). Finally, if a 5GDHC system is compared vs conventional cooling solutions, the overall local impact on UHIs is not only the one related to pure anthropogenic heat (i.e., chiller electricity consumptions), but the one related to the entire cooling thermal power (as explained for Ospitaletto).

## 5 Aalborg case

Aalborg is a city located in the north of Denmark. It has a population of about 120,000 inhabitants, considering the proper town only; Aalborg municipality extends over a large territory and totals to about 140,000 inhabitants overall. Most of the city is reached by a conventional district heating network, largely supplied by waste heat (from a big cement factory) and combined heat and power plants (CHP), mainly burning coal.

Aalborg has a maritime climate, with short, mild summers and long, moderately cold winters. The mean daily maximum temperature in summer is about 21 °C, with a record high temperature of the order of 35 °C. The mean daily minimum temperature in winter is about -2 °C, with a record low temperature of about -26 °C. Precipitation is rather evenly distributed along the year, with values between 30 and 70 mm every month.

As proved by the large development of wind turbines, Aalborg is characterized by large wind amounts. This contributes to strong circulation effects which prevent the formation of significant UHIs in the city. The city is split by the Limfjord, a shallow part of the sea separating the North Jutlandic Island from the rest of the Jutland Peninsula. Aalborg therefore includes a harbour area with an extended waterfront. The presence of the sea also contributes to the mild and ventilated climate.

Given this situation and having already observed that even for the climate of Ospitaletto the UHI effect related to heating and cooling anthropogenic contributions is very small, no detailed investigation was carried out for this northern case. The waste heat recovery activities demonstrated in the LIFE4HeatRecovery project might further improve the sustainability of the Aalborg district heating network (already quite efficient, but still employing significant amounts of coal for its CHP plants), but without a direct impact on local temperatures. Moreover, cooling penetration is expected to remain limited. Hence, no significant impact on the local climatic conditions can be expected from heating and cooling technologies.



## 6 References

- Almeida, Sofia, Elsa Casimiro, and Antonis Analitis (2013). “Short-term effects of summer temperatures on mortality in Portugal: a time-series analysis”. In: *Journal of Toxicology and Environmental Health, Part A* 76.7, pp. 422–428.
- Andreou, Andreas et al. (2020). “Decomposing the drivers of residential space cooling energy consumption in EU-28 countries using a panel data approach”. In: *Energy and Built Environment*.
- Arnfield, A John (2003). “Two decades of urban climate research: a review of turbulence, exchanges of energy and water, and the urban heat island”. In: *International Journal of Climatology: a Journal of the Royal Meteorological Society* 23.1, pp. 1–26.
- Bechtel, Benjamin et al. (2015). “Mapping local climate zones for a worldwide database of the form and function of cities”. In: *ISPRS International Journal of Geo-Information* 4.1, pp. 199–219.
- Bhatt, Kanishk Pratimkumar (2016). “THE IMPACT OF BUILDINGS IN THEIR SURROUNDING MICROCLIMATES: THE CASE OF MANDEVILLE AND HORSENDEN SCHOOLS.”
- Borghi, G. (2020). “Analysis of the Urban Heat Island effect in Ospitaletto (BS) and of the mitigation potential provided by waste heat recovery measures”. Master thesis, Università di Trento.
- Chen, Chi-Feng (2013). “Performance evaluation and development strategies for green roofs in Taiwan: A review”. In: *Ecological engineering* 52, pp. 51–58.
- Chen, Fei et al. (2011). “The integrated WRF/urban modelling system: development, evaluation, and applications to urban environmental problems”. In: *International Journal of Climatology* 31.2, pp. 273–288.
- Darmanto, Nisrina Setyo et al. (2019). “Future urban climate projection in a tropical megacity based on global climate change and local urbanization scenarios”. In: *Urban Climate* 29, p. 100482.
- Dipasquale, C et al. (2014). “D2. 1c simulation results of reference buildings”. In: EC FP7 project iNSPiRe, Grant agreement 314461.
- Dipasquale, Chiara et al. (2019). “Database of energy, environmental and economic indicators of renovation packages for European residential buildings”. In: *Energy and Buildings* 203, p. 109427.
- Florens, Emma, Olivier Eiff, and Frédéric Moulin (2013). “Defining the roughness sublayer and its turbulence statistics”. In: *Experiments in fluids* 54.4, pp. 1–15.
- Grimmond, CSB and Timothy R Oke (2002). “Turbulent heat fluxes in urban areas: Observations and a local-scale urban meteorological parameterization scheme (LUMPS)”. In: *Journal of Applied Meteorology* 41.7, pp. 792–810.
- Hove, Bert van et al. (2010). *Modelling and observing urban climate in the Netherlands*. KvR report number: KvR 020/11.
- Kim, Yeon-Hee and Jong-Jin Baik (2005). “Spatial and temporal structure of the urban heat island in Seoul”. In: *Journal of Applied Meteorology* 44.5, pp. 591–605.
- Klok, L. et al. (2010). “Ruimtelijke verdeling en mogelijke oorzaken van het hitte-eiland effect” (Spatial distribution and possible causes of the heat island effect), TNO-034-UT-2010-01229.
- Martilli, Alberto, Alain Clappier, and Mathias W Rotach (2002). “An urban surface exchange parameterisation for mesoscale models”. In: *Boundary-layer meteorology* 104.2, pp. 261–304.

- Nuruzzaman, Md (2015). "Urban heat island: causes, effects and mitigation measures- a review". In: International Journal of Environmental Monitoring and Analysis 3.2, pp. 67–73.
- Oke, TR (1988). "The urban energy balance". In: Progress in Physical geography 12.4, pp. 471–508.
- Oke, TR (1976). "The distinction between canopy and boundary-layer urban heat islands". In: Atmosphere 14.4, pp. 268–277.
- Oke, TR (1982). "The energetic basis of the urban heat island". In: Quarterly Journal of the Royal Meteorological Society 108.455, pp. 1–24.
- Oke, TR and HA Cleugh (1987). "Urban heat storage derived as energy balance residuals". In: Boundary-Layer Meteorology 39.3, pp. 233–245.
- Othmer, Felix Julian, Jörg Peter Schmitt, and Stefan Greiving (2020). "Numerical modelling of the urban climate as an integrated part of environmental assessments". In: Science of The Total Environment 731, p. 138774.
- Program, Energy Sector Management Assistance (2020). Primer for Cool Cities: Reducing Excessive Urban Heat—With a Focus on Passive Measures.
- Ribeiro, I et al. (2021). "Highly resolved WRF-BEP/BEM simulations over Barcelona urban area with LCZ". In: Atmospheric Research 248, p. 105220.
- Rizwan, Ahmed Memon, Leung YC Dennis, and LIU Chunho (2008). "A review on the generation, determination and mitigation of Urban Heat Island". In: Journal of Environmental Sciences 20.1, pp. 120–128.
- Robinson, Peter J (2001). "On the definition of a heat wave". In: Journal of applied Meteorology 40.4, pp. 762–775.
- Rosenzweig, Cynthia E, John Antle, and Joshua Elliott (2015). "Assessing impacts of climate change on food security worldwide".
- Sailor, David J and Chittaranjan Vasireddy (2006). "Correcting aggregate energy consumption data to account for variability in local weather". In: Environmental Modelling & Software 21.5, pp. 733–738.
- Salamanca, Francisco et al. (2018). "Evaluation of the WRF-urban modeling system coupled to Noah and Noah-MP land surface models over a semiarid urban environment". In: Journal of Geophysical Research: Atmospheres 123.5, pp. 2387–2408.
- Santamouris, Matheos (2016). "Cooling the buildings—past, present and future". In: Energy and Buildings 128, pp. 617–638.
- Santamouris, Matheos et al. (2001). "On the impact of urban climate on the energy consumption of buildings". In: Solar energy 70.3, pp. 201–216.
- Skamarock, WC, JB Klemp, and J Dudhia (2008). "A Description of the Advanced Research WRF Version 3. NCAR/TN-475+STR. National Center for Atmospheric Research".
- Stewart, Ian D and Tim R Oke (2012). "Local climate zones for urban temperature studies". In: Bulletin of the American Meteorological Society 93.12, pp. 1879–1900.
- Ürge-Vorsatz, Diana et al. (2015). "Heating and cooling energy trends and drivers in buildings". In: Renewable and Sustainable Energy Reviews 41, pp. 85–98.
- Wang, Y Q (2014). "MeteoInfo: GIS software for meteorological data visualization and analysis". In: Meteorological Applications 21.2, pp. 360–368.

Woodward, Alistair et al. (2014). "Climate change and health: on the latest IPCC report". In: The Lancet 383.9924, pp. 1185–1189.

Zonato, A et al. (2020). "Evaluating the performance of a novel WUDAPT averaging technique to define urban morphology with mesoscale models". In: Urban Climate 31, p. 100584.

Zonato, Andrea (2016). "Evaluating the Urban Heat Island for cities of Emilia-Romagna region through numerical simulations" Master thesis, Università di Bologna.